

# Distributed SIMO Physical Layer Authentication: Performance Bounds Under Optimal Attacker Strategies

Henrik Forssell<sup>✉</sup>, *Student Member, IEEE*, Ragnar Thobaben<sup>✉</sup>, *Member, IEEE*,

## Abstract

We provide worst-case bounds for the detection performance of a physical layer authentication scheme where authentication is based on channel-state information (CSI) observed at multiple distributed remote radio-heads (RRHs). The bounds are established based on two physical-layer attack strategies that a sophisticated attacker can launch against a given deployment. First, we consider a power manipulation attack, in which a single-antenna attacker adopts optimal transmit power and phase, and derive an approximation for the missed detection probability that is applicable for both statistical and perfect CSI knowledge at the attacker. Secondly, we characterize the spatial attack position that maximizes the attackers success probability under strong line-of-sight conditions. We use this to provide a heuristic truncated search algorithm that efficiently finds the optimal attack position, and hence, constitutes a powerful tool for planning, analyzing, and optimizing deployments. Interestingly, our results show that there is only a small gap between the detection performance under a power manipulation attack based on statistical respectively perfect CSI knowledge, which significantly strengthens the relevance and applicability of our results in real-world scenarios. Furthermore, our results illustrate the benefits of the distributed approach by showing that the worst-case bounds can be reduced by 4 orders of magnitude without increasing the total number of antennas.

## Index Terms

Manuscript submitted May 10, 2020. This work was supported in part by the Swedish Civil Contingencies Agency, MSB, through the CERCES project. The authors want to thank professor James Gross for discussions and insights that contributed to the completion of this work as well as for proof-reading the final manuscript. H. Forssell and R. Thobaben are with the School of Electrical Engineering and Computer Science, KTH Royal Institute of Technology, Stockholm, Sweden (e-mail: hefo@kth.se; ragnart@kth.se).

## I. INTRODUCTION

Authentication at the physical (PHY) layer of wireless communications is currently researched as a means of providing enhanced security in applications where quick authentication with low complexity and security overhead is desirable. For instance, PHY-layer security techniques have been considered for ultra-reliable low-latency communications (URLLC) to provide security guarantees even when the room for security overhead and authentication delays is slim-to-none [1, 2]. PHY-layer authentication (PLA) can in such a setting be an effective way to detect and filter out sophisticated impersonation attacks, which otherwise could degrade the communication performance and harm the underlying applications.

The core idea of feature-based PLA is to verify the legitimacy of a message by exploiting characteristic features of the user locations or hardware chipsets that can be inferred from the received PHY-layer signals. The idea was first introduced in [3] and has since then been studied in various contexts such as vehicular networks [4], wireless sensor networks [5], and lately, also in URLLC [2, 6, 7]. Several different PHY-layer features have been employed, ranging from hardware-specific features such as local oscillator offsets [8], offsets in clock frequencies [9], and switching transients [10], to location-specific features such as the received signal strength [11], the wide band multi-path channel [3], and multiple-antenna channels [12, 13]. The big advantage of feature-based PLA is that it requires no additional security overhead, as opposed to cryptographic authentication and tag-based PLA that rely on embedding a pre-agreed secret key [14]. This can relieve higher layer protocols from some of the complex key generation and distribution tasks while still maintaining the message integrity. Key-based approaches are known to be vulnerable to eavesdropping (e.g., covertness is crucial for a tag-based PLA scheme [14]) and are easily broken if legitimate keys should leak to an attacker. The feature-based approach, on the other hand, does not suffer from these problems. The use of diverse features and combinations of features such as, for example, the channel-state information in a multiple antenna system renders the estimation and impersonation of the legitimate feature a very challenging task for an attacker.

However, there are also partly unresolved problems related to the feature-based PLA approach: One problem, that has not received much attention, is that an attacker can use various smart strategies to mimic the legitimate user features. For instance, carrier frequency offsets can be

impersonated by adapting the transmit frequency to match the legitimate transmitter's, and RSSIs can be altered by manipulating the transmit power. With PLA based on more diverse channel features, an attacker can use pre-coding based on correlated observations to optimally mimic the legitimate channel feature [13]. Moreover, with the use of location-specific features the question arises, what is an optimal attack position to mimic the legitimate channel. Apart from the work in [13, 15–17], performance analysis of PLA under such attacker strategies has not been extensively studied in previous literature.

Moreover, despite its apparent benefits for the URLLC setting, PLA also introduces system-level costs due to erroneous authentication decisions. These erroneous decisions, stemming from the underlying hypothesis tests (i.e., false alarms and missed detections), might have several unwanted consequences in a mission-critical application like delays due to false alarms or security breaches due to missed detections. For this reason, when considering the use of PLA for mission-critical communication scenarios like URLLC, the concepts of security, reliability, and latency become closely connected. Broadly speaking, for a given choice of authentication threshold, an appropriate PLA scheme must be able to provide two types of guarantees: Firstly, that the system-level delay impacts of the authentication scheme are kept within certain limits, a problem we have studied in our previous works [18–20]; and secondly, that the probability of a successful attack is guaranteed to be below a certain threshold regardless of the attacker's capabilities.

In this paper, we develop tools for providing guarantees of the second type. To that end, we propose to extend array-based PLA to the distributed network setting where multiple remote radio-heads (RRHs) forward their messages to a centralized processing unit (see as well [19]), and derive worst-case detection bounds of the system. This distributed system model is motivated by communication techniques such as distributed MIMO and coordinated multi-point (CoMP). Authentication is here based on the single-input multiple-output (SIMO) channel states whose distributions in turn depend on the transmitter's physical location (i.e., distance and angle-of-arrival) with respect to the RRHs. To bound the worst-case missed detection probability, in this paper we define and analyze two PHY-layer attack strategies: (i) a power manipulation attack, where the attacker adapts power and phase at its single-antenna transmitter in order to shape its channel response by scaling and phase rotation, and (ii) an optimal position attack, where the attacker chooses the spatial position so as to optimize her success probability.

The main contributions of this paper are: We propose and analyze the performance of feature-based PLA in a wireless network with multiple distributed RRHs. We derive the optimal transmit-

power manipulation strategy under perfect channel-state information (CSI) knowledge and the corresponding worst-case missed detection probability that serves as a worst-case bound for a given attacker location, given in closed-form for a single RRH and as a saddle-point approximation for the multiple RRH case. We provide an approximation of the missed detection probability under any power manipulation strategy, and in particular, for a strategy that only requires statistical CSI knowledge. We characterize the optimal attacker position with respect to a given network deployment under strong line-of-sight assumptions and provide a heuristic truncated search algorithm that significantly reduces the search-space to a set of locally optimal attack positions.

The rest of this paper is organized as follows: Section II introduces the considered system model, authentication scheme, and the problem formulation. In Section III, we analyze the power manipulation attack and provide the corresponding missed detection probabilities. In Section IV, we study the optimal attacker positions and define the heuristic optimization approach. Section V provides the numerical evaluation of the derived performance bounds and compares different deployment strategies. Finally, the paper is concluded in Section VI.

*Notation:* Matrices are represented by bold capital symbols  $\mathbf{X}$ , and  $\mathbf{X}^T$  and  $\mathbf{X}^\dagger$  denote the matrix transpose and conjugate transpose, respectively. We let  $\mathbf{I}$  denote the identity matrix. Vectors with entries  $x_i$  are represented by bold lower-case symbols  $\mathbf{x}$  for which we let  $\|\mathbf{x}\| = \sqrt{|x_1|^2 + \dots + |x_n|^2}$  denote the Euclidian norm and  $\|\mathbf{x}\|_{\mathbf{A}}^2 = \mathbf{x}^\dagger \mathbf{A} \mathbf{x}$  denote the complex quadratic form. We use  $F_X(x)$  to represent the cumulative distribution function of a random variable  $X$ . We let  $\mathcal{CN}(\boldsymbol{\mu}, \boldsymbol{\Sigma})$  represent the multivariate proper complex Gaussian distribution with mean  $\boldsymbol{\mu}$  and covariance matrix  $\boldsymbol{\Sigma}$ ,  $\mathcal{N}(\boldsymbol{\mu}, \boldsymbol{\Sigma})$  the corresponding real-valued Gaussian distribution,  $\chi_k^2$  a central  $\chi^2$  distribution with  $k$  degrees of freedom, and  $\chi_k^2(\lambda)$  a non-central  $\chi^2$  distribution with  $k$  degrees of freedom and non-centrality parameter  $\lambda$ .

## II. SYSTEM MODEL AND PRELIMINARIES

In this paper, we analyze authentication of uplink transmissions in a wireless system running a mission-critical application (e.g., sensors sending data to an industrial automation process). As depicted in Fig. 1, we consider a distributed system architecture consisting of  $N_{\text{RRH}}$  remote radio-heads (RRHs), each equipped with  $N_{\text{RX}}$  receive antennas, connected to a centralized baseband processor we refer to as Bob. There is a legitimate stationary single-antenna sensor device referred to as Alice (A) and a rouge device, referred to as Eve (E), attempting to compromise the system

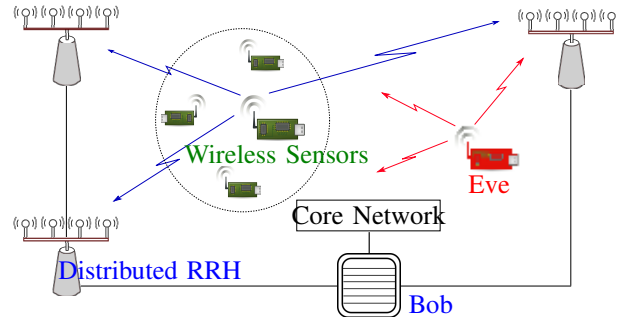


Fig. 1. System deployment consisting of wireless sensors communicating in uplink to multiple-antenna remote radio-heads (RRHs), a centralized baseband processor (Bob) connected to the core network, and an adversary (Eve) equipped with wireless sensor hardware.

by impersonating Alice. The PHY layer authentication scheme considered in this paper, which will be formally introduced in Section II-B, is designed to protect the system against Eve’s impersonation attempts by comparing the CSI of each transmission against a pre-stored feature bank. The rest of this section provides detailed descriptions of the system model assumptions, the authentication scheme and its error probabilities, and the considered PHY-layer attack strategies available to Eve.

#### A. System Model Assumptions

The uplink transmissions are assumed to be organized in periodic frames using time-division multiple-access (TDMA). Each frame consists of a broadcast beacon, followed by a management period (MGMT) and a data transmission period (DTP). In the MGMT period devices can request connecting to the access point (CN), disconnecting (DCN), or resources for transmission of data payload (DTA). The MGMT period is assumed to be based on low-rate transmissions and contention access; however, we assume that collisions and decoding errors are handled appropriately such that we can neglect their impact.

The MAC protocol discussed here is open to certain vulnerabilities. Here, we summarize three particular vulnerabilities that motivate the need for PLA: (i) a data injection attack where an attacker sends DTA requests impersonating a legitimate device which allows it to transmit false data into the core network; (ii) a disassociation attack where an attacker sends fake DCN requests which allows it to interrupt a legitimate device’s transmission by temporarily disconnecting it; (iii) a Sybil attack where an attacker sends multiple DTA requests with multiple device IDs which, due to the limited resources in a frame, reduces the amount of resources available for legitimate devices.

Generally, one might assume that MGMT requests and DTA transmissions would be encrypted and authenticated through cryptographic means. However, in a network with many sensors and simultaneous strict requirements on latency, the overhead due to cryptographic key-agreement and distribution might not be manageable. Moreover, any given encryption scheme can be broken if keys somehow were to leak to the attacker.

The PHY-layer channels from the devices to the RRHs are modeled as narrowband single-input multiple-output (SIMO) channels centered at frequency  $f_c$  and subject to Rice fading. Thus, our model assumes that each link has a significant line-of-sight (LoS) component to each RRH, and therefore, the CSI statistics depend on both the angle-of-arrival (AoA) and distance with respect to each receive array. We let  $\mathbf{h}_i^{(j)}$  denote the  $(N_{\text{Rx}} \times 1)$  complex channel vector from device  $i = \{A, E\}^1$  to array  $j$  and model them as circular-symmetric complex Gaussian (CSCG) vectors  $\mathbf{h}_i^{(j)} \sim \mathcal{CN}(\boldsymbol{\mu}_i^{(j)}, \boldsymbol{\Sigma}_i^{(j)})$  (i.e., narrowband SIMO Rice fading), where we let  $\boldsymbol{\mu}_i^{(j)}$  and  $\boldsymbol{\Sigma}_i^{(j)}$  denote the corresponding mean vector and covariance matrix, respectively. We assume that  $\mathbb{E}[\|\mathbf{h}_{i,j}^{(j)}\|^2] = P_i^{(j)} N_{\text{Rx}}$  where  $P_i^{(j)}$  represents the average power received per antenna and that the covariance matrices take the form  $\boldsymbol{\Sigma}_i^{(j)} = \frac{P_i^{(j)}}{K_{\text{Rice}} + 1} \boldsymbol{\Lambda}$ , where  $\boldsymbol{\Lambda}$  is a fixed correlation matrix identical for each RRH. This assumption of equal fading correlation for antennas within an RRH is reasonable under the assumption that the arrays have the same geometry and that they are deployed in a homogenous environment. We use a parametric model for the received power per antenna  $P_i^{(j)} = \left(\frac{\lambda_c}{4\pi d_i^{(j)}}\right)^\beta P_{\text{Tx},i}$ , with  $\lambda_c = c/f_c$  being the wavelength,  $d_i^{(j)}$  the distance,  $P_{\text{Tx},i}$  the transmit power, and  $\beta$  a path-loss exponent (i.e.,  $\beta = 2$  represents free-space path loss). Note also that we deliberately let both transmit power and path-loss be parts of the CSI vectors  $\mathbf{h}_i^{(j)}$  through  $P_i^{(j)}$  since the receiver in practice is unable to differentiate these from each other based on the received signals.

Finally, we adopt a phased-array model of the expected value of the channels which then becomes a location-specific statistic of the channel distributions. We denote by  $\Phi_i^{(j)}$  the spatial angle-of-arrival from transmitter  $i$  w.r.t. array  $j$  and let

$$\boldsymbol{\mu}_i^{(j)} = \sqrt{\frac{P_i^{(j)} K_{\text{Rice}}}{K_{\text{Rice}} + 1}} \times e^{-\frac{j2\pi d_i^{(j)}}{\lambda_c}} \mathbf{e}(\Omega_i^{(j)}), \quad (1)$$

<sup>1</sup>Note that the model presented in this section extends to multiple devices  $i = 1, \dots, N_{\text{devices}}$ ; however, in this paper we only consider the single legitimate device Alice.

where the array-response vector  $\mathbf{e}(\Omega) = [1, e^{-j2\pi\Delta_r\Omega}, \dots, e^{-j2\pi\Delta_r(N_{\text{Rx}}-1)\Omega}]^T$  is modeling the phase differences between antenna elements in terms of the angular sine  $\Omega = \sin(\Phi)$  and normalized antenna separation  $\Delta_r$ .

In the following section, we define the PLA scheme based on the model assumptions of this section that provides an additional layer of security and effectively can detect and filter out the above-mentioned MAC-layer attacks.

### B. Physical Layer Authentication Scheme

In this paper, we consider the authentication problem where Bob receives a message  $m$  with uncertainty as to whether it originated from Alice or Eve. We assume that the message is intercepted by every RRH and we denote by  $\tilde{\mathbf{h}}_m^{(j)} = \text{CSI}(m)$  the observed channel-state vector at receive array  $j$ . We denote by  $\mathcal{H}_0$  the hypothesis that the message is from Alice, i.e., that  $\tilde{\mathbf{h}}_m^{(j)} = \mathbf{h}_A^{(j)}$ , and by  $\mathcal{H}_1$  the hypothesis that it is from Eve, i.e., that  $\tilde{\mathbf{h}}_m^{(j)} = \mathbf{h}_E^{(j)}$ . In general,  $\tilde{\mathbf{h}}_m^{(j)}$  would be a channel-state estimate with limited precision; however, to simplify the analysis in the following we assume perfect CSI at the RRHs. We note, however, that parts of our results generalize to imperfect CSI and refer to Section III-C for additional details.

Bob's objective is to centrally decide whether to accept the message or not based on information received from the RRHs. For that purpose, we construct the  $(N_{\text{Rx}}N_{\text{RRH}} \times 1)$  CSI vector  $\tilde{\mathbf{h}}_m = [[\tilde{\mathbf{h}}_m^{(1)}]^T \dots [\tilde{\mathbf{h}}_m^{(N_{\text{RRH}})}]^T]^T$ . Given that the message is authentic (i.e.,  $\mathcal{H}_0$  is true), we have  $\tilde{\mathbf{h}}_m \sim \mathcal{CN}(\boldsymbol{\mu}_A, \boldsymbol{\Sigma}_A)$ , with

$$\boldsymbol{\mu}_A = \begin{bmatrix} \boldsymbol{\mu}_A^{(1)} \\ \vdots \\ \boldsymbol{\mu}_A^{(N_{\text{RRH}})} \end{bmatrix} \quad \text{and} \quad \boldsymbol{\Sigma}_A = \begin{bmatrix} \boldsymbol{\Sigma}_A^{(1)} & \mathbf{0} & \dots & \mathbf{0} \\ \mathbf{0} & \boldsymbol{\Sigma}_A^{(2)} & \dots & \mathbf{0} \\ \vdots & \vdots & \ddots & \vdots \\ \mathbf{0} & \mathbf{0} & \dots & \boldsymbol{\Sigma}_A^{(N_{\text{RRH}})} \end{bmatrix}, \quad (2)$$

where the diagonal structure of  $\boldsymbol{\Sigma}_A$  follows from the assumption of independent fading across RRHs. Now let us introduce the authentication test which is based on the generalized likelihood-ratio test (GLRT) often used in related work on PLA [3, 13, 21]:

*Definition 1 (Authentication Hypothesis Test): Bob makes an acceptance decision according to the following binary hypothesis test:*

$$d(\tilde{\mathbf{h}}_m) \underset{\mathcal{H}_0}{\overset{\mathcal{H}_1}{\geq}} T, \quad (3)$$

where  $d(\cdot)$  is a discriminant function associated with the channel feature of Alice, given by

$$d(\tilde{\mathbf{h}}_m) = 2\|\tilde{\mathbf{h}}_m - \boldsymbol{\mu}_A\|_{\Sigma_A^{-1}}^2. \quad (4)$$

In some cases, the CSI might only be locally available at the RRHs and not centrally available at Bob. However, note that by defining  $d^{(j)}(\tilde{\mathbf{h}}) = 2\|\tilde{\mathbf{h}}^{(j)} - \boldsymbol{\mu}_A^{(j)}\|_{\{\Sigma_A^{(j)}\}^{-1}}^2$  we can write the discriminant function in (3) as  $d(\tilde{\mathbf{h}}_m) = \sum_{j=1}^{N_{\text{RRH}}} d^{(j)}(\tilde{\mathbf{h}}_m^{(j)})$ , which holds due to the block diagonal structure of the covariance matrix  $\Sigma_A$ . That is, in practice (3) can be used even if the RRHs only communicate their individual soft decisions  $d_i^{(j)}(\tilde{\mathbf{h}})$  which can be summed up at Bob, rather than communicating the entire CSI vector  $\tilde{\mathbf{h}}$ .

*Discussion:* Note that prior to using the PLA scheme, Bob must initially learn the legitimate statistics  $\boldsymbol{\mu}_A^{(j)}, \Sigma_A^{(j)}$ . This is an important problem as well as a common observation in related PLA literature, where it is often argued that the initial trust is established using cryptographic authentication whenever a new transmitter joins the network [17]. Another solution in our scenario would be to use device position information to infer the corresponding channel statistics from the model (1). Such an approach could also encompass device mobility by allowing the legitimate feature bank to be time-varying. However, the details of such methods are considered outside the scope of this work, and we presuppose that Bob (or at least the RRHs) knows the time-invariant  $\boldsymbol{\mu}_i^{(j)}, \Sigma_i^{(j)}$  perfectly.

### C. Error Probabilities

Two types of errors can occur in the binary authentication test (3): Type-I error (i.e., false alarm) when a legitimate message is rejected, and Type-II (i.e., missed detection) when an adversary message is accepted. The probability of false alarm and missed detection are defined as  $p_{\text{FA}}(T) = \mathbb{P}(d(\tilde{\mathbf{h}}_m) > T | \mathcal{H}_0)$  and  $p_{\text{MD}}(T) = \mathbb{P}(d(\tilde{\mathbf{h}}_m) < T | \mathcal{H}_1)$ , respectively. It is easy to show that  $d(\tilde{\mathbf{h}}_m) | \mathcal{H}_0 \sim \chi_{2N_{\text{RRH}}N_{\text{Rx}}}^2$ , i.e., the discriminant function is following a central  $\chi^2$  distribution. Hence, the false alarm probability can be obtained in closed form according to  $p_{\text{FA}}(T) = 1 - F_{\chi_{2N_{\text{RRH}}N_{\text{Rx}}}^2}(T)$ . The missed detection probability  $p_{\text{MD}}(T)$  is generally not straightforwardly tractable in the multiple RRH case since  $d(\tilde{\mathbf{h}}_m) | \mathcal{H}_1$  is a weighted sum of non-central  $\chi^2$  variables. However, we have previously provided an efficient approximation in [19].

### D. PHY-Layer Attack Strategies

Now we introduce the PHY attack strategies that our worst-case bounds in Section III and IV are based on.



*Definition 2 (PHY Layer Attack 1: Power Manipulation): Eve manipulates the transmit power and phase at her single-antenna transmitter by employing a complex scaling factor  $\rho_E e^{j\varphi_E}$  such that the channel state observed at Bob becomes  $\eta_E e^{j\psi_E} \mathbf{h}_E$ . Eve can adopt either a fixed power manipulation strategy based on statistical CSI or a channel-realization dependent strategy based on perfect CSI at Eve.*

*Definition 3 (PHY Layer Attack 2: Attack Position): Eve chooses her spatial position with respect to the receive arrays to influence the statistics of her channel distribution. The objective for Eve is to find the optimal position, i.e., the one that maximizes the missed detection probability with respect to the legitimate device position and the RRH deployment.*

These strategies can be launched by external entities (e.g., an attacker positioned in close proximity to the system, using a stolen device or a software defined radio unit) or internal devices whose behavior has been hijacked by malicious code. Obviously, these attacks can also be combined with MAC-layer attacks such as disassociation or Sybil attacks to maximize the attack impact.

#### *E. Problem Formulation*

For the considered PLA scheme, the tradeoff between the false alarm probability and the missed detection probability is controlled by the authentication threshold  $T$ . In a mission-critical scenario, these probabilities will influence system-level performance (i.e., packet-drops, delays, etc.) most obviously through the false alarms that cause packet-drops and potentially re-transmissions. In such contexts, worst-case bounds in the form  $p_{\text{MD}}(T) < p_{\text{MD}}^{(\text{Worst-Case})}$  can prove exceptionally useful, since they allow Bob to confidently set the highest possible threshold  $T$  (that is causing the minimal amount of false alarms) while still maintaining a guaranteed detection performance. Providing such bounds and investigating how various design-choices influence them is the aim of this work. Section III is devoted to analyzing this problem under the optimal power manipulation attack while Section IV provides solutions under the optimal position attack.

### III. POWER MANIPULATION ATTACK

In this section, we provide a worst-case missed detection performance analysis under the optimal power manipulation attack. Recall that under a power manipulation strategy, Eve manipulates power and phase, modeled by complex scaling factor  $\eta_E e^{j\psi_E}$ , with the objective to maximize the success probability given by the probability of missed detection  $p_{\text{MD}}(T)$ . First, we will derive the optimal strategy under the assumption that Eve has perfect knowledge of her instantaneous

CSI and provide an approximation of the associated missed detection probability. Next, we will introduce a strategy based on only statistical CSI knowledge and provide the missed detection probability under this assumption.

#### A. Optimal Attack Given Perfect CSI at Eve

Here, we assume that Eve perfectly knows the channel states  $\mathbf{h}_E^{(j)}$  with respect to each RRH, prior to her impersonation attempt. This might be considered an unrealistically competent attacker; however, it is relevant since the missed detection probability under this assumption will serve as a worst-case upper bound for any power manipulation strategy. Considering that the missed detection probability under the power manipulation attack is defined by  $p_{MD}(T) = \mathbb{P}(d(\eta_E e^{j\psi_E} \mathbf{h}_E) < T)$ , the optimal strategy will be to minimize the discriminant function  $d(\eta_E e^{j\psi_E} \mathbf{h}_E)$  given by (4). That strategy is provided in the following lemma:

*Lemma 1 (Optimal Power Manipulation Attack Given Perfect CSI): The power manipulation strategy that minimizes the discriminant function (4) is given by*

$$\eta_E^* = \frac{|\boldsymbol{\mu}_A^\dagger \boldsymbol{\Sigma}_A^{-1} \mathbf{h}_E|}{\mathbf{h}_E^\dagger \boldsymbol{\Sigma}_A^{-1} \mathbf{h}_E}, \quad \psi_E^* = -\arg\{\boldsymbol{\mu}_A^\dagger \boldsymbol{\Sigma}_A^{-1} \mathbf{h}_E\}, \quad (5)$$

yielding the minimal achievable lower bound on the discriminant function  $d(\mathbf{h}_E) \geq d^{(Opt. PMA)}$  where

$$d^{(Opt. PMA)} = 2\boldsymbol{\mu}_A^\dagger \boldsymbol{\Sigma}_A^{-1} \boldsymbol{\mu}_A \left( 1 - \frac{|\boldsymbol{\mu}_A^\dagger \boldsymbol{\Sigma}_A^{-1} \mathbf{h}_E|^2}{\boldsymbol{\mu}_A^\dagger \boldsymbol{\Sigma}_A^{-1} \boldsymbol{\mu}_A \mathbf{h}_E^\dagger \boldsymbol{\Sigma}_A^{-1} \mathbf{h}_E} \right). \quad (6)$$

*Proof.* See Appendix A. □

Strategy (5) allows us to formulate an upper bound for the detection performance in the following definition:

*Definition 4 (Detection Performance Under Optimal Power Manipulation Attack):*

$$p_{MD} \leq p_{MD}^{(Opt. PMA)} \triangleq \mathbb{P}(d^{(Opt. PMA)} < T) = \mathbb{P}\left(\frac{|\boldsymbol{\mu}_A^\dagger \boldsymbol{\Sigma}_A^{-1} \mathbf{h}_E|^2}{\boldsymbol{\mu}_A^\dagger \boldsymbol{\Sigma}_A^{-1} \boldsymbol{\mu}_A \mathbf{h}_E^\dagger \boldsymbol{\Sigma}_A^{-1} \mathbf{h}_E} > 1 - \frac{T}{2\boldsymbol{\mu}_A^\dagger \boldsymbol{\Sigma}_A^{-1} \boldsymbol{\mu}_A}\right). \quad (7)$$

To provide insight into the problem of evaluating (7), we define  $t = 1 - \frac{T}{2\boldsymbol{\mu}_A^\dagger \boldsymbol{\Sigma}_A^{-1} \boldsymbol{\mu}_A}$ ,  $\mathbf{z} = \frac{\mathbf{Q}_A \boldsymbol{\mu}_A}{\|\mathbf{Q}_A \boldsymbol{\mu}_A\|}$ , and  $\bar{\mathbf{h}}_E = \mathbf{Q}_E^\dagger \mathbf{h}_E$ , where  $\mathbf{Q}_i$  is the Cholesky factorization of  $\boldsymbol{\Sigma}_i^{-1}$  for  $i = \{A, E\}$ . With some manipulation (7) can be re-written in terms of a quadratic form

$$p_{MD}^{(Opt. PMA)}(T) = \mathbb{P}(\bar{\mathbf{h}}_E^\dagger \mathbf{A}(t) \bar{\mathbf{h}}_E > 0) \quad (8)$$

where  $\mathbf{A}(t) = \mathbf{Q}_E^{-1} \mathbf{Q}_A^\dagger (\mathbf{z} \mathbf{z}^\dagger - t \mathbf{I}) \mathbf{Q}_A (\mathbf{Q}_E^{-1})^\dagger$ .

Note that the determinant  $|\mathbf{A}(t)| = |\Sigma_E||\Sigma_A^{-1}||\mathbf{z}\mathbf{z}^\dagger - t\mathbf{I}| = |\Sigma_E||\Sigma_A^{-1}|(-t)^{N-1}(1-t)$  which implies that, if  $t > 0$  and the total number of antennas  $N = N_{\text{RRH}}N_{\text{Rx}}$  is even,  $|\mathbf{A}(t)| < 0$  and  $\mathbf{A}(t)$  will have an odd number of negative eigenvalues. Hence, the probability  $p_{\text{MD}}^{(\text{Opt. PMA})}(T)$  generally takes the form of the complementary CDF of an indefinite quadratic form in the complex Gaussian vector  $\bar{\mathbf{h}}_E \sim \mathcal{CN}(\mathbf{b}, \mathbf{I})$  with  $\mathbf{b} = \mathbf{Q}_E^\dagger \mu_E$ . Closed-form expressions for such distributions are generally not tractable; however, several approximation methods exist in the literature. In the following, we provide two efficient methods that can be used for evaluating the probability (7). First, we solve the problem in closed-form in Theorem 1 for the single-array case ( $N_{\text{RRH}} = 1$ ) by exploiting the particular structure of the matrix  $\mathbf{A}(t)$ . Then we generalize the result to multiple arrays in Theorem 2 ( $N_{\text{RRH}} > 1$ ) based on a previously developed approximation for CDFs of indefinite quadratic forms [22].

*a) Solution for  $N_{\text{RRH}} = 1$ :* In the case of a single receive array, the worst-case missed detection probability can be evaluated in closed-form. The reason is that under the assumption  $N_{\text{RRH}} = 1$ , we can analytically find the eigenvalues of the matrix  $\mathbf{A}$ , which allows us to write the statistic as a ratio of two  $\chi^2$  random variables. This ratio, by definition, follows a doubly non-central F-distribution for which closed-form distribution functions exist in the literature. We formulate this result in the following theorem:

*Theorem 1 (Single-Array Worst-Case Missed Detection Probability): For a single receive array ( $N_{\text{RRH}} = 1$ ), the worst-case missed detection probability can be obtained in closed form*

$$p_{\text{MD}}^{(\text{Opt. PMA})}(T) = 1 - F_{\text{DNCF}}(x; \nu_1, \nu_2, k_1, k_2) \quad (9)$$

where  $x = (N_{\text{Rx}} - 1) \left(1 - \frac{2\mu_A^\dagger \Sigma_A^{-1} \mu_A}{T}\right)$ ,  $\nu_1 = \frac{2|\mu_A^\dagger \Sigma_A^{-1} \mu_E|^2}{\alpha \mu_A^\dagger \Sigma_A^{-1} \mu_A}$ ,  $\nu_2 = \frac{2}{\alpha} \left(\mu_E^\dagger \Sigma_A^{-1} \mu_E - \frac{|\mu_A^\dagger \Sigma_A^{-1} \mu_E|^2}{\mu_A^\dagger \Sigma_A^{-1} \mu_A}\right)$ ,  $k_1 = 2$ ,  $k_2 = 2(N_{\text{Rx}} - 1)$ , and

$$F_{\text{DNCF}}(x; \nu_1, \nu_2, k_1, k_2) = e^{-\frac{\nu_1 + \nu_2}{2}} \sum_{r=0}^{\infty} \sum_{s=0}^{\infty} \frac{\left(\frac{\nu_1}{2}\right)^r}{r!} \frac{\left(\frac{\nu_2}{2}\right)^s}{s!} I\left(\frac{k_1 x}{k_2 + k_1 x}; \frac{n_1}{2} + r, \frac{n_2}{2} + s\right) \quad (10)$$

denotes the CDF of a doubly non-central F-distribution with non-centrality parameters  $\nu_1$  and  $\nu_2$ , degrees of freedom  $k_1$  and  $k_2$ , written in terms of the incomplete beta function  $I(q; a, b) = \int_0^q t^{a-1}(1-t)^{b-1}dt$ .

*Proof.* We start from (7), but instead define  $\bar{\mathbf{h}}_E = \mathbf{Q}_A \mathbf{h}_E$  where  $\mathbf{Q}_A$  again is the Cholesky factorization of  $\Sigma_A^{-1}$ . Using this, we can continue from (7) and write

$$p_{\text{MD}}^{(\text{wc})}(T) = \mathbb{P}\left(\frac{|\mathbf{z}^\dagger \bar{\mathbf{h}}_E|^2}{\|\bar{\mathbf{h}}_E\|^2} > t\right) = \mathbb{P}\left(\bar{\mathbf{h}}_E^\dagger \mathbf{z}^\dagger \mathbf{z} \bar{\mathbf{h}}_E > t \bar{\mathbf{h}}_E^\dagger \bar{\mathbf{h}}_E\right) = \mathbb{P}(\bar{\mathbf{h}}_E^\dagger (\mathbf{z}^\dagger \mathbf{z} - t\mathbf{I}) \bar{\mathbf{h}}_E > 0). \quad (11)$$

The matrix  $\mathbf{A}_2 = \mathbf{z}^\dagger \mathbf{z} - t\mathbf{I}$  is clearly Hermitian which means that we can write  $\mathbf{A}_2 = \mathbf{U}^\dagger \mathbf{D} \mathbf{U}$  where  $\mathbf{D}$  is a real-valued diagonal matrix with the eigenvalues  $d_i = -t$  for  $i = 1, \dots, N_{\text{Rx}} - 1$  and  $d_{N_{\text{Rx}}} = 1 - t$  and  $\mathbf{U}$  is an orthonormal matrix with the last column equal to  $\mathbf{z}$ . Now since  $\Sigma_E = \alpha \Sigma_A$ , we can let  $\mathbf{x} \triangleq \mathbf{U} \bar{\mathbf{h}}_E = \mathbf{U} \mathbf{Q}_A \mathbf{h}_E \sim \mathcal{CN}(\mathbf{U} \mathbf{Q}_A \boldsymbol{\mu}_E, \alpha \mathbf{I})$ ,  $X_1 \triangleq |x_{N_{\text{Rx}}}|^2 \sim \frac{2}{\alpha} \chi_2^2 \left( \frac{2}{\alpha} |[\mathbf{U} \mathbf{Q}_A \boldsymbol{\mu}_E]_{N_{\text{Rx}}}|^2 \right)$ , and

$$X_2 \triangleq \sum_{i=1}^{N_{\text{Rx}}} |x_i|^2 \sim \frac{2}{\alpha} \chi_{2(N_{\text{Rx}}-1)}^2 \left( \frac{2}{\alpha} \sum_{i=1}^{N_{\text{Rx}}} |[\mathbf{U} \mathbf{Q}_A \boldsymbol{\mu}_E]_i|^2 \right), \quad (12)$$

which are independent due to the independence of the elements in  $\mathbf{x}$ . Based on these definitions we find that

$$\begin{aligned} \mathbb{P}(\bar{\mathbf{h}}_E^\dagger (\mathbf{z}^\dagger \mathbf{z} - t\mathbf{I}) \bar{\mathbf{h}}_E > 0) &= \mathbb{P}(\mathbf{x}^\dagger \mathbf{D} \mathbf{x} > 0) = \mathbb{P} \left( (1-t)|x_{N_{\text{Rx}}}|^2 - t \sum_{i=1}^{N_{\text{Rx}}} |x_i|^2 > 0 \right) \\ &= \mathbb{P} \left( \frac{|x_{N_{\text{Rx}}}|^2}{\sum_{i=1}^{N_{\text{Rx}}} |x_i|^2} > \frac{t}{1-t} \right) = \mathbb{P} \left( \frac{\frac{X_1}{2}}{\frac{X_2}{2(N_{\text{Rx}}-1)}} > (N_{\text{Rx}}-1) \frac{t}{1-t} \right). \end{aligned} \quad (13)$$

The lefthand-side ratio  $Y \triangleq \frac{\frac{X_1}{2}}{\frac{X_2}{2(N_{\text{Rx}}-1)}}$  in (13) is therefore a ratio of normalized independent  $\chi^2$  random variables which by definition follows a doubly non-central F-distribution. Hence,  $p_{\text{MD}}^{(\text{wc})}(T) = \mathbb{P}(Y > (N_{\text{Rx}}-1) \frac{t}{1-t})$  from which the result in (9) follows.  $\square$

*b) Saddle-Point Approximation for  $N_{\text{RRH}} > 1$ :* In the multiple-array case,  $\mathbf{A}$  will generally not possess the Hermitian property that was exploited in Theorem 1. Therefore, we instead turn to integral approximation techniques. Using the eigenvalue decomposition  $\mathbf{A} = \mathbf{U} \mathbf{D} \mathbf{U}^\dagger$  and a strategy similar to the one proposed in [22], the probability (7) can be transformed into a one-dimensional integral, for any real-valued parameter  $\beta > 0$ , stated in the following proposition

*Proposition 1 (Alternative Formulation of Worst-Case Missed Detection Probability):*

$$p_{\text{MD}}^{(\text{Opt. PMA})} = -\frac{1}{2\pi} \int_{-\infty}^{\infty} \frac{e^{-c(\omega)}}{(\beta - j\omega) |\mathbf{I} + (\beta - j\omega) \mathbf{D}|} d\omega, \quad (14)$$

with the arbitrary real constant  $\beta > 0$ ,  $\mathbf{b} = \mathbf{Q}_E^\dagger \boldsymbol{\mu}_E$ , and

$$c(\omega) = \mathbf{b}^\dagger \left( \mathbf{I} + \frac{1}{j\omega - \beta} \mathbf{D}^{-1} \right)^{-1} \mathbf{b}. \quad (15)$$

*Proof.* See Appendix B.  $\square$

Although neither this integral is computable in closed form, it is easier to handle than the brute force  $N_{\text{RRH}} N_{\text{Rx}}$ -dimensional integral over the CSCG vector  $\mathbf{h}$ . Here we use a saddle-point method to approximate the integral (14) in the following theorem:

*Theorem 2 (Approximation of Worst-Case Missed Detection Probability for  $N_{\text{Rx}} \geq 2$ ): The worst-case missed detection probability can be approximately evaluated as*

$$p_{\text{MD}}^{(\text{Opt. PMA})} \approx -\frac{1}{2\pi} e^{s(z_0)} e^{-j\angle s''(z_0)} \sqrt{\frac{2\pi}{|s''(z_0)|}}, \quad (16)$$

where

$$s(z) = -\mathbf{b}^\dagger \left( \mathbf{I} + \frac{1}{z} \mathbf{D}^{-1} \right)^{-1} \mathbf{b} - \ln(z) - \ln(|\mathbf{I} + z\mathbf{D}|), \quad (17)$$

$\mathbf{b} = \mathbf{Q}_E^\dagger \boldsymbol{\mu}_E$ , and  $z_0$  is a stationary point such that  $s'(z_0) = 0$ .

*Proof.* With a change to the complex variable  $z = j\omega - \beta$ , we can write (14) as

$$p_{\text{MD}}^{(wc)} = -\frac{1}{j2\pi} \oint_{-\beta-j\infty}^{-\beta+j\infty} e^{-s(z)} dz \quad (18)$$

with  $s(z)$  defined according to (17). The saddle point method uses the approximation  $s(z) \approx s(z_0) + \frac{1}{2}s''(z_0)(z - z_0)^2$  to write

$$\begin{aligned} p_{\text{MD}}^{(wc)} &\approx -\frac{1}{j2\pi} \oint_{-\beta-j\infty}^{-\beta+j\infty} e^{-(s(z_0) + \frac{1}{2}s''(z_0)(z-z_0)^2)} dz \\ &= -\frac{1}{j2\pi} e^{-s(z_0)} \oint_{-\beta-j\infty}^{-\beta+j\infty} e^{-\frac{1}{2}s''(z_0)(z-z_0)^2} dz = -\frac{1}{j2\pi} e^{-s(z_0)} e^{j\phi} \sqrt{\frac{2\pi}{|s''(z_0)|}} \end{aligned} \quad (19)$$

with  $\phi = \frac{\pi - \angle s''(z_0)}{2}$ . Finally, we note that  $e^{j\phi} = j e^{-j\angle s''(z_0)}$  from which (16) follows.  $\square$

### B. Fixed Power Manipulation Strategy (Statistical CSI at Eve)

Suppose now that Eve can only choose a fixed strategy for  $\eta_E e^{j\psi_E}$ , i.e., one that does not depend on the instantaneous CSI  $\mathbf{h}_E$ . For example, Eve can choose a strategy based on knowledge of  $\boldsymbol{\mu}_A$  and  $\boldsymbol{\mu}_E$ , which in practice could be obtained by using ray-tracing tools. For any fixed strategy, we can clearly formulate the missed detection probability as

$$p_{\text{MD}}^{(\text{Fixed PMA})}(T) = \mathbb{P}(\|\eta_E e^{j\psi_E} \mathbf{h}_E - \boldsymbol{\mu}_A\|_{\Sigma_A^{-1}}^2 < T/2) \quad (20)$$

Note that we have  $\eta_E e^{j\psi_E} \mathbf{h}_E - \boldsymbol{\mu}_A \sim \mathcal{CN}(\boldsymbol{\mu}, \Sigma)$  with  $\boldsymbol{\mu} = \eta_E e^{j\psi_E} \boldsymbol{\mu}_E - \boldsymbol{\mu}_A$  and  $\Sigma = \eta_E^2 \Sigma_E$ , so the probability (20) again takes the form of a CDF of a complex Gaussian quadratic form. Hence, we can calculate (20) by using the following corollary to Theorem 2:

*Corollary 1: For the fixed power manipulation strategy, we get  $p_{\text{MD}}^{(\text{Fixed PMA})}(T)$  by replacing  $\bar{\mathbf{h}}_E$  with  $\eta_E e^{j\psi_E} \mathbf{h}_E - \boldsymbol{\mu}_A$  in (8) and apply the saddle-point approximation as described in Theorem 2.*

Note that the approach in Corollary 1 also allows us to evaluate the missed detection probability without power manipulation attack by letting  $\eta_E = 1$  and  $\psi_E = 0$ .

Finally, in the following definition we provide a special case of fixed strategy when Eve has only statistical CSI knowledge:

*Definition 5* (Power Manipulation Attack Based On Statistical CSI):

$$\eta_E^{(stat)} = \frac{|\boldsymbol{\mu}_A^\dagger \boldsymbol{\Sigma}_A^{-1} \boldsymbol{\mu}_E|}{\boldsymbol{\mu}_E^\dagger \boldsymbol{\Sigma}_A^{-1} \boldsymbol{\mu}_E}, \quad \psi_E^{(stat)} = -\arg\{\boldsymbol{\mu}_A^\dagger \boldsymbol{\Sigma}_A^{-1} \boldsymbol{\mu}_E\}, \quad (21)$$

The motivation behind strategy (21) is to use the strategy derived in Lemma 1 but assume the strong LoS approximation  $\mathbf{h}_E \approx \boldsymbol{\mu}_E$ .

### C. Generalization to Imperfect CSI

The analysis provided thus far has assumed perfect CSI at Bob; however, a generalization to i.i.d. CSI estimation noise is possible by extending  $\boldsymbol{\Sigma}_i^{(j)} = \frac{P_i^{(j)}}{K_{\text{Rice}}+1} \boldsymbol{\Lambda} + \sigma_n^2 \mathbf{I}$ , where  $\sigma_n^2$  is the estimation noise variance. Note that under this assumption, the saddle-point approximation in Theorem 2 applies straightforwardly, while the closed-form solution in Theorem 1 only applies under the assumption of uncorrelated antennas  $\boldsymbol{\Lambda} = \mathbf{I}$ . Due to space limitations, we have not included estimation errors in the system model or in our numerical results, and the impact of estimation errors is left for future studies.

## IV. OPTIMAL ATTACK POSITION

In this section, we study the problem of finding the optimal attack position with respect to a given deployment. We will denote Alice's and Eve's spatial positions by  $\xi_A$  and  $\xi_E$ , respectively, and assume that Eve knows the deployment and position of the legitimate device. Obviously, a straightforward solution for optimizing  $p_{\text{MD}}^{(\text{Opt. PMA})}(\xi_E)$  is to pick  $\xi_A = \xi_E$  which will result in  $p_{\text{MD}}^{(\text{Opt. PMA})} = 1 - p_{\text{FA}}$ . However, a basic underlying assumption is that the attacker is significantly separated from the legitimate device since the authentication method in-itself is predicated on this spatial separation in order to work. Therefore, here we rather seek locally optimal attacker positions that are outside the immediate neighborhood of the legitimate device. We start with defining and characterizing the objective function and identify properties of local optima that we exploit in our heuristic search algorithm. The algorithm is then presented in Section IV-E.

### A. General Optimization Problem

The optimal attack position is equivalent to the one maximizing  $p_{\text{MD}}^{(\text{Opt. PMA})}(\xi_E) = \mathbb{P}(d^{(\text{Opt. PMA})}(\mathbf{h}_E) < T)$ , that is, the worst-case position given that Eve is using the optimal power manipulation attack.

Straightforwardly, from rearranging (7), this problem can be rewritten in a convenient form, as stated in the following definition:

*Definition 6 (Optimal Position Attack): We define the region of allowed attack positions as  $\mathcal{R}$  and let  $\boldsymbol{\mu}_E(\xi_E), \boldsymbol{\Sigma}_E(\xi_E)$  denote the channel statistics induced by the attack position  $\xi_E \in \mathcal{R}$ . The optimal attack position is given as the solution to*

$$\xi_E^* = \arg \max_{\xi_E \in \mathcal{R}} \mathbb{P}(F_{obj}(\mathbf{h}_E) > T^*), \quad (22)$$

where

$$F_{obj}(\mathbf{h}_E) = \frac{|\boldsymbol{\mu}_A^\dagger \boldsymbol{\Sigma}_A^{-1} \mathbf{h}_E|^2}{\mathbf{h}_E^\dagger \boldsymbol{\Sigma}_A^{-1} \mathbf{h}_E} \quad (23)$$

is an objective function and  $T^* = \boldsymbol{\mu}_A^\dagger \boldsymbol{\Sigma}_A^{-1} \boldsymbol{\mu}_A - T/2$  is a constant threshold.

Direct optimization of (22) results in a very complicated optimization problem due to the somewhat complicated distribution of (23).

#### B. Characterization of Objective Function Under Strong LoS Assumption

First, let us consider the case of strong LoS conditions, i.e., when  $K_{\text{Rice}}$  is large and  $\mathbf{h}_E \approx \boldsymbol{\mu}_E(\xi_E)$ . In such a setting, the objective function in (23) is approximately  $F_{obj}(\boldsymbol{\mu}_E(\xi_E))$ . Under these assumptions, our approach is to expand (23) to provide an understanding of how the missed detection probability depends on the attack position. First, we introduce some notation related to the positions of Alice and Eve with respect to the RRHs that will prove useful: We define the distance ratios  $r_j = \frac{d_A^{(j)}}{d_E^{(j)}}$ , the phase offsets  $\varphi_E^{(j)} = \frac{2\pi d_E^{(j)}}{\lambda_c}$  and  $\varphi_A^{(j)} = \frac{2\pi d_A^{(j)}}{\lambda_c}$ , phase differences  $\Delta\varphi_j = \varphi_E^{(j)} - \varphi_A^{(j)}$ , and angular-sine differences  $\Delta\Omega_j = \Omega_E^{(j)} - \Omega_A^{(j)}$ . Furthermore, we define the per-array inner products of the angular responses as

$$S_{ik}^{(j)} = \mathbf{e}(\Omega_i^{(j)})^\dagger \boldsymbol{\Lambda}^{-1} \mathbf{e}(\Omega_k^{(j)}), \quad (24)$$

for  $i, k \in \{\text{A}, \text{E}\}$ .

For certain correlation matrices, we can additionally expand the inner products  $S_{EA}^{(j)}$  according to the following lemma:

*Lemma 2: For any correlation matrix with inverse in the form  $\boldsymbol{\Lambda}^{-1} = \mathbf{T} + \mathbf{M}$ , where  $\mathbf{T}$  is a symmetric Toeplitz matrix defined by the first column  $[t_0, \dots, t_{N-1}]^T$  and  $\mathbf{M}$  is a diagonal matrix with  $[\mathbf{M}]_{k,l} = m_0$  for  $k = l = 2, \dots, N-1$  (i.e., all diagonal elements equal except the first and last one being zero), we have*

$$S_{EA}^{(j)} = e^{j2\pi \frac{N_{Rx}-1}{2} \Delta_r \Delta \Omega_j} g(\Omega_E^{(j)}), \quad (25)$$

where  $g(\Omega_E^{(j)})$  is a real-valued function.

*Proof.* The sum along the main diagonal in  $\mathbf{T}$  will take the form  $\sum_{n=0}^{N_{Rx}-1} t_0 e^{j2\pi \Delta_r \Delta \Omega_j n}$ , which possesses the property in (25) according to exponential sum formulas. This property extends to all the remaining diagonals in  $\mathbf{T}$  and  $\mathbf{M}$  but the details are left out due to space limitations.  $\square$

Based on these definitions, we provide the expanded representation of  $F_{\text{obj}}(\boldsymbol{\mu}_E(\xi_E))$  in the following lemma:

*Lemma 3* (Expanded Objective Function):

$$F_{\text{obj}}(\boldsymbol{\mu}_E(\xi_E)) = K_{\text{Rice}} \left| \frac{\sum_{j=1}^{N_{RRH}} \sqrt{\bar{r}_j} |g(\Omega_E^{(j)})| e^{j\phi_0^{(j)}}}{\sqrt{\sum_{j=1}^{N_{RRH}} \bar{r}_j S_{EE}^{(j)}}} \right|^2 \quad (26)$$

with  $\phi_0^{(j)} = \Delta\varphi_j + 2\pi \frac{N_{Rx}-1}{2} \Delta_r \Delta \Omega_j + \frac{\pi}{2} [\text{sign}\{g(\Omega_E^{(j)})\} - 1]$  and  $\bar{r}_j = \frac{r_j^\beta}{\sum_l^{N_{RRH}} r_l^\beta}$  where  $\beta$  is the path-loss exponent.

*Proof.* We obtain (26) by expanding (23) using the block diagonal structure of  $\Sigma_A$ , the definitions of  $\boldsymbol{\mu}_E$  and  $\boldsymbol{\mu}_A$  according to (1), and the result in Lemma 2.  $\square$

By inspecting (26), we can make two key observations that we will later exploit in Section IV-E:

- 1) Small-scale optimization of  $F_{\text{obj}}(\boldsymbol{\mu}_E(\xi_E))$  depends on the complex coefficients  $e^{j\phi_0^{(j)}}$  related to the phase-relation of transmissions received at each RRH.
- 2) Large-scale optimization depends on the angular responses  $|g(\Omega_E^{(j)})|$  and the normalized distance ratios  $\bar{r}_k$ .

### C. Impact of Fading Correlation

In addition to the general result in Lemma 2, we provide the angular response  $g(\Delta\Omega_j)$  in closed form under two special cases, summarized in the two following lemmas:

*Lemma 4* (Uncorrelated Antennas): *Given the assumption of uncorrelated antennas ( $\boldsymbol{\Lambda} = \mathbf{I}$ ), we have*

$$g(\Delta\Omega_j) = \frac{\sin(\pi \Delta_r N_{Rx} \Delta\Omega_j)}{N_{Rx} \sin(\pi \Delta_r \Delta\Omega_j)} \quad (27)$$

*Proof.* This follows from the conceptual proof of Lemma 2 with  $t_0 = 1$  and  $t_i = 0$  for  $i > 0$ .  $\square$



*Lemma 5: For the exponential correlation matrix  $\mathbf{\Lambda}_{k,l} = \rho^{-|k-l|}$ , we have*

$$\begin{aligned} g(\Delta\Omega_j) &= \frac{1}{(1 - \rho^2) \sin(\pi\Delta_r\Delta\Omega_j)} \\ &\times [\sin(\pi\Delta_r N_{Rx}\Delta\Omega_j) + \rho^2 \sin(\pi\Delta_r(N_{Rx} - 2)\Delta\Omega_j) \\ &- 2\rho \cos(\pi\Delta_r(\Omega_{E,k} + \Omega_{A,k})) \sin(\pi\Delta_r(N_{Rx} - 1)\Delta\Omega_j)]. \end{aligned} \quad (28)$$

*Proof.* The inverse of the exponential correlation matrix is a Toeplitz matrix with  $t_0 = \frac{1}{1-\rho^2}$ ,  $t_1 = \frac{\rho^2}{1-\rho^2}$ ,  $t_2 = \frac{-2\rho}{1-\rho^2}$ , and  $t_i = 0$  for  $i > 2$ . The rest follows from the same idea as in the proof of Lemma 2.  $\square$

*D. Characterization of Locally Optimal Attack Positions for Uncorrelated Antenna Fading and  $N_{RRH} = 2$*

To simplify the analysis, we assume a deployment of two RRHs and uncorrelated antenna fading. In the case of uncorrelated antenna fading, it is easy to find that  $S_{EE}^{(j)} = 1$  and, thus, we have  $\sum_{k=1}^{N_{RRH}} \bar{r}_k S_{EE}^{(j)} = 1$ . Moreover, with the assumption of  $N_{RRH} = 2$ , we can write the expanded objective function as

$$F_{\text{obj}}(\boldsymbol{\mu}_E(\xi_E)) = \left| \sqrt{\bar{r}_1} |g(\Delta\Omega_1)| e^{j\phi_0^{(1)}} + \sqrt{\bar{r}_2} |g(\Delta\Omega_2)| e^{j\phi_0^{(2)}} \right|^2. \quad (29)$$

The aforementioned small-scale local optima allow us to reduce the optimization search to a set of spatial sampling points for which we have a specific phase relation as specified in the following lemma:

*Lemma 6 (Small-Scale Spatial Sampling  $N_{RRH} = 2$ ): The small-scale local optima of  $F_{\text{obj}}(\boldsymbol{\mu}_E(\xi_E))$  are found at points where  $e^{j\phi_0^{(1)}} = e^{j\phi_0^{(2)}}$ . At such points we have*

$$F_{\text{obj}}(\boldsymbol{\mu}_E(\xi_E)) = (\sqrt{\bar{r}_1} |g(\Delta\Omega_1)| + \sqrt{\bar{r}_2} |g(\Delta\Omega_2)|)^2. \quad (30)$$

*Proof.* Clearly, the norm of (29) is maximized when  $\arg(\sqrt{\bar{r}_k} |g(\Delta\Omega_k)| e^{j\phi_0^{(k)}}) = \phi_0^{(j)} = \phi_0$  for both RRHs.  $\square$

*Remark 1: Lemma 6 generalizes to  $N_{RRH} > 2$  by considering points where  $e^{j\phi_0^{(1)}} = e^{j\phi_0^{(2)}} = \dots = e^{j\phi_0^{(N_{RRH})}}$ . However, note that the existence of points with optimal phase alignment with respect to more than two arrays at a time is not guaranteed and depends on the RRH deployment and Alice's position.*

Now let us restrict the angular sine differences to the set  $\Delta\Omega \in \mathcal{A}$ , where  $\mathcal{A}$  is a set of local optima of the angular response  $|g(\Delta\Omega)|$ .

*Remark 2:* Note that for RRH  $j$ , we have  $\Delta\Omega = \sin(\Phi_E^{(j)}) - \sin(\Phi_A^{(j)})$  which implies that each local optima  $\Delta\Omega \in \mathcal{A}$  is associated with two attack angles  $\Phi_E^{(j,+)} = \sin^{-1}(\Delta\Omega + \sin(\Phi_A^{(j)}))$  and  $\Phi_E^{(j,-)} = \pi - \Phi_E^{(j,+)}$ .

Now we can characterize the large-scale local optima in the following theorem:

*Theorem 3 (Large-Scale Local Optima for  $N_{\text{RRH}} = 2$  arrays):* At far-field points where  $\bar{r}_k$  remain approximately constant in the local neighborhood, large-scale local optima of  $F_{\text{obj}}(\boldsymbol{\mu}_E(\xi_E))$  are found at the intersection points of the set lines with AoAs associated with angular sines  $\Delta\Omega \in \mathcal{A}$ .

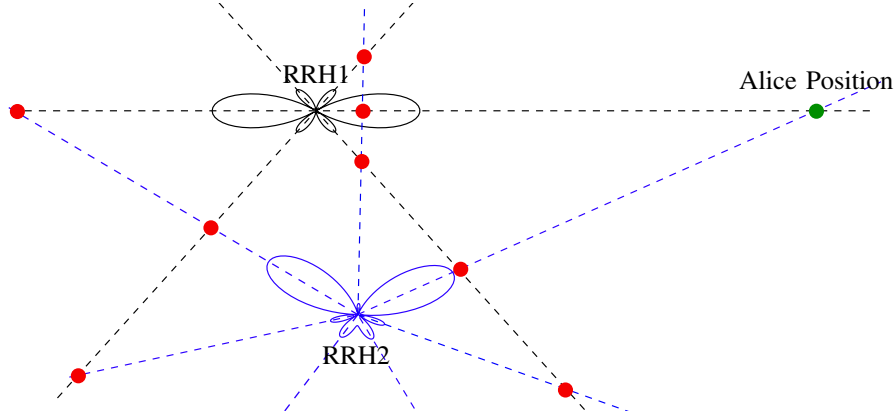


Fig. 2. Illustration of candidate points for optimal attacker position with  $N_{\text{RRH}} = 2$  RRHs. Dashed lines indicate the rays with AoA  $\Phi_{E,l}^*$ .

*Proof.* Lets choose two particular angular sines  $\Delta\Omega_1, \Delta\Omega_2 \in \mathcal{A}$ . Let  $\xi_E^*$  denote the intersection point between the lines<sup>2</sup> with AoAs  $\Phi_E^{(1,+)}$  and  $\Phi_E^{(2,+)}$ . Now from the definition of  $\mathcal{A}$ , we know that  $|g(\Delta\Omega_k + \epsilon_k)| < |g(\Delta\Omega_k)|$  for  $k = 1, 2$  and  $\epsilon_k$  sufficiently small so that we stay in the neighborhood of the local optima of  $g(\cdot)$ . Clearly, if we deviate from  $\xi_E^*$  to a point  $\xi_E'$  with any angle offsets  $\epsilon_1$  and  $\epsilon_2$ , where the deviation is small such that  $\bar{r}_k$  is approximately constant, then we see that

<sup>2</sup>Generally, such an intersection point might not exist; however, for the proof of this theorem we assume that  $\Delta\Omega_1$  and  $\Delta\Omega_2$  are chosen such that it does.

$$F_{\text{obj}}(\boldsymbol{\mu}_{\text{E}}(\xi_{\text{E}}')) = K_{\text{Rice}} \left( \sqrt{r_1} |g(\Delta\Omega_1 + \epsilon_1)| + \sqrt{r_2} |g(\Delta\Omega_2 + \epsilon_2)| \right)^2 \quad (31)$$

$$< K_{\text{Rice}} \left( \sqrt{r_1} |g(\Delta\Omega_1)| + \sqrt{r_2} |g(\Delta\Omega_2)| \right)^2 = F_{\text{obj}}(\boldsymbol{\mu}_{\text{E}}(\xi_{\text{E}}^*)), \quad (32)$$

which shows that  $\xi_{\text{E}}^*$  is a large-scale local optima of  $F_{\text{obj}}(\boldsymbol{\mu}_{\text{E}}(\xi_{\text{E}}))$ .  $\square$

Fig. 2 provides an illustration of the intersection points considered in Theorem 3.

The analysis thus far provides us with characterizations of small- and large-scale locally optimal points under certain assumptions. In the final part of this section, we will exploit these results to develop a heuristic truncated search algorithm that can be used to find the optimal attack position in the general case efficiently.

### E. Heuristic Search Method for General Deployments and Rice Fading

Our proposed search method can be summarized as follows: (i) In accordance with Theorem 3, reduce the search to points where AoAs are within the main lobe of a RRH or intersections of 1<sup>st</sup> order side-lobes. (ii) Based on Lemma 6, use the function  $F_{\text{small-scale}}(\xi_{\text{E}})$  defined below to find small-scale locally optimal points. (iii) Compute the missed detection probability  $p_{\text{MD}}^{(\text{Opt. Position})}$  for the truncated set of small-scale local optima from step (ii).

The search algorithm is based on the following definitions: We let

$$F_{\text{small-scale}}(\xi_{\text{E}}) = \left| \sum_{k=1}^{N_{\text{RRH}}} e^{j\phi_0^{(j)}(\xi_{\text{E}})} \right| \quad (33)$$

be a small-scale optimization function for finding small-scale locally optimal points and let  $B(\xi_{\text{E}}, \epsilon)$  define the set of points within distance  $\epsilon$  from attack position  $\xi_{\text{E}}$ . For RRH  $j$ , the main lobe AoAs are  $\Phi_{\text{main}}^{(j)} = \{\Phi_A^{(k)}, \pi - \Phi_A^{(k)}\}$  and we let  $\Phi_{1^{\text{st}}}^{(j)}$  denote the first side lobe AoA (local maxima) of the angular response. Based on this, the sets of searched AoA are defined as  $\mathcal{A}_{\text{main}}^{(j)} = [\Phi_{\text{main}}^{(j)} - \delta_-, \Phi_{\text{main}}^{(j)} + \delta_+]$  where  $\delta_{+/-}$  is chosen such that  $\left| g \left( \sin(\Phi_{\text{main}}^{(j)}) - \sin(\Phi_A^{(k)}) \right) \right| = g_0 \left| g \left( \sin(\Phi_{\text{main}}^{(j)} \pm \delta) - \sin(\Phi_A^{(k)}) \right) \right|$ , for a constant  $g_0$ . The AoA search set for the first side lobe  $\mathcal{A}_{1^{\text{st}}}^{(j)}$  is similarly defined. Based on these definitions, Algorithm 1 describes the steps of the search method in mathematical detail. In related work, sometimes the main lobe beam width is defined as  $2/L_r$  where  $L_r = \lambda_c \Delta_r N_{\text{Rx}}$  represents the array length. This definition can also be used in our problem, but note that the parametric choice based on  $g_0$  is more general as it allows us to tune the beam width considered in the search.

---

**Algorithm 1** Truncated Search: Critical Attack Positions

---

```
1: procedure FINDOPTIMALATTACKPOSITION( $\mathcal{R}$ ) ▷ Search allowed region  $\mathcal{R}$ 
2:   for  $j = 1, \dots, N_{\text{RRH}}$  do
3:      $\mathcal{P} \leftarrow \{\xi_E \in \mathcal{R}; \Phi_E^{(j)} \in \mathcal{A}_{\text{main}}^{(j)}\}$  ▷ Mainlobes
4:     for  $k = 1, \dots, N_{\text{RRH}}$  and  $k \neq j$  do
5:        $\mathcal{P} \leftarrow \mathcal{P} \cup \{\xi_E \in \mathcal{R}; \Phi_E^{(j)} \in \mathcal{A}_{1^{\text{st}}}^{(j)} \wedge \Phi_E^{(k)} \in \mathcal{A}_{1^{\text{st}}}^{(k)}\}$  ▷ Intersect. of sidelobes
6:     end for
7:      $\mathcal{P}_{\text{Critical}}(j) \leftarrow \{\xi_E \in \mathcal{P}; F_{\text{small-scale}}(\xi_E) \geq F_{\text{small-scale}}(\xi) \forall \xi \in B(\xi_E, \epsilon)\}$ 
8:     ▷ Restrict to small-scale local optima
9:   end for
10:   $p_{\text{MD}}^{(\text{Opt. Position})} = \max_{\xi_E \in \bigcup_{j=1}^{N_{\text{RRH}}} \mathcal{P}_{\text{Critical}}(j)} p_{\text{MD}}^{(\text{Opt. PMA})}(\xi_E)$ 
11: end procedure
```

---

At a first glance, it may appear as an arbitrary choice to restrict the search to the main lobes and intersections of 1<sup>st</sup> order side lobes. However, the structure of the maxima of the angular responses in Lemma 4 and 5 induces a decreasing hierarchy of side lobe maxima. Unfortunately, an analytical characterization of the objective function with respect to the impact of the local maxima of  $g(\cdot)$  is difficult, since distances change with intersection points as well. However, our numerical results presented in the next section confirm that it is sufficient to restrict the search to intersections of first-order side lobes since local optima of higher order side lobes are inferior.

## V. NUMERICAL RESULTS

In this section, we numerically study the detection performance under the considered attack strategies for different distributed network topologies. We consider a system deployed in a 80 m×60 m area, as depicted in Fig. 3. In the area there are 9 potential RRH locations RRH1-RRH9 where antenna arrays of varying sizes can be placed, a legitimate device Alice, and the attacker Eve. For all the subsequent results, we assume that the normalized antenna separation  $\Delta_r = 0.5$ , the path-loss exponent  $\beta = 2$ , and that the system operates at  $f_c = 2.4$  GHz center frequency. Moreover, for the following results the authentication threshold  $T$  is fixed for  $p_{\text{FA}} = 10^{-2}$  unless stated otherwise.

### A. Validation of Saddle-Point Approximation

In Fig. 4 and 5, we validate the approximation of the missed detection probability (MDP) under the power manipulation attack for a variety of parameter choices and compare the results

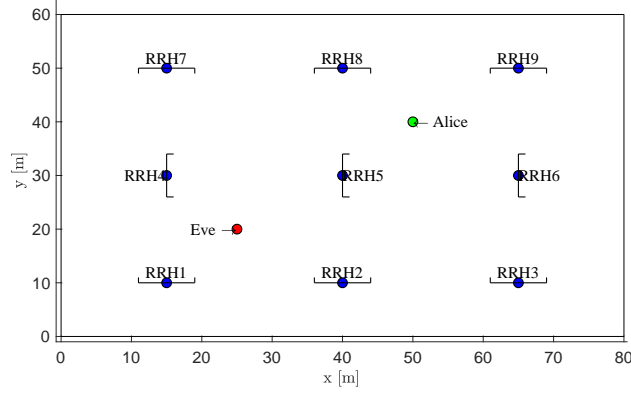


Fig. 3. The 80 m×60 m network deployment area used for numerical evaluations: 9 fixed RRH locations A1-A9, legitimate transmitter device Alice, and the attacker Eve.

to Monte-Carlo simulations. We plot the missed detection probability both under optimal power manipulation, i.e.,  $p_{\text{MD}}^{(\text{Opt. PMA})}$  and without power manipulation. The curves represent the evaluation of the saddle-point approximation in Theorem 2, and the Monte-Carlo simulation results, indicated by the cross markers, are computed based on  $10^7$  channel realizations sampled from CSCG distributions. The results are based on a deployment of  $N_{\text{RRH}} = 3$  RRHs (RRH locations 1, 3, and 8) with  $N_{\text{Rx}} = 2$  antennas each. Alice and Eve are located at  $\xi_A = (65 \text{ m}, 30 \text{ m})$  and  $\xi_E = (26 \text{ m}, 49 \text{ m})$ , respectively.

The first thing to note from Fig. 4 and 5 is that the proposed saddle-point approximation provides accurate results for all parameter ranges. Small approximation errors can be observed which generally seem to upper bound the true values obtained from the Monte Carlo simulations.

Fig. 4(a) shows the missed detection probability for varying false alarm probabilities (i.e., this is the receiver operating characteristic curve for varying choices of threshold  $T$ ). Observe that Eve gains significantly (i.e., several orders of magnitude) in success probability by using the optimal attack strategy. Fig. 4(b) shows the same missed detection probabilities but for varying total number of receive antennas where we can see that the missed detection probability generally decreases with the number of antennas as expected.

In Fig. 5(a), we plot the missed detection probability as Eve moves along the  $x_E$ -axis with fixed  $y_E = 49 \text{ m}$ , illustrating that the detection performance is varying with small variations in attacker position. Fig. 5(b) illustrates the missed detection probability for varying values of the fading correlation coefficient  $\rho$ . We generally observe a decreasing missed detection probability as the magnitude  $|\rho|$  increases. Note that the fading correlation coefficient  $\rho$  represents the correlation in the channel fading; i.e.,  $\rho = 0$  represents independent fading across antennas and

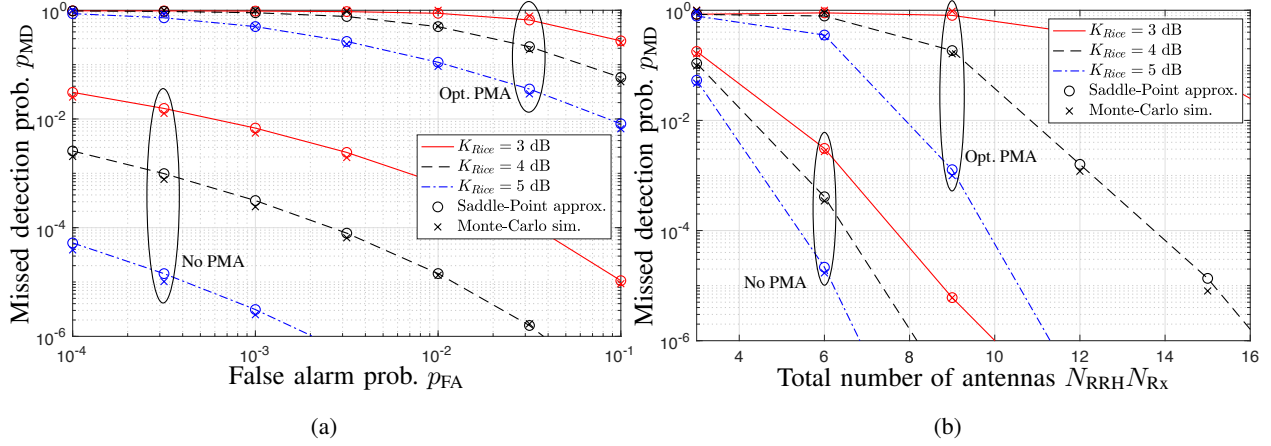


Fig. 4. Saddle-point approximation of  $p_{MD}^{(Opt. PMA)}$  compared to Monte-Carlo simulations for a  $N_{RRH} = 3$  RRH deployment for: (a) different false alarm probabilities and (b) varying total number of deployed antennas  $N_{RRH}N_{Rx}$ .

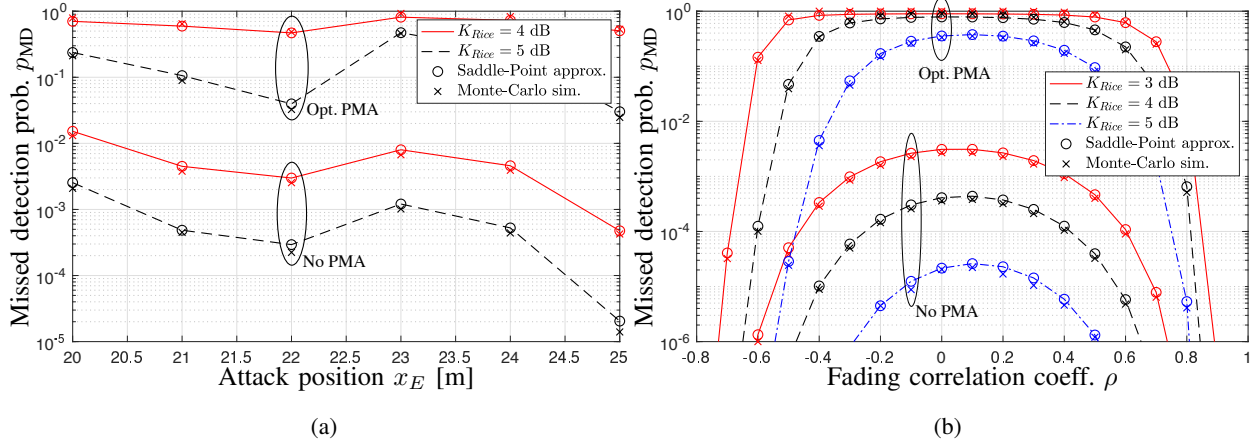


Fig. 5. Saddle-point approximation of  $p_{MD}^{(Opt. PMA)}$  compared to Monte-Carlo simulations for a  $N_{RRH} = 3$  RRH deployment for: (a) small variations in Eve's position and (b) varying correlation coefficient  $\rho$ .

$\rho = 1$  represents full correlation. From Fig. 4 and 5, we can also observe that the detection performance increases (missed detection probability decreases) with increasing Rice factor  $K_{Rice}$  as expected.

### B. Impacts of Power Manipulation Attack

In Fig. 6, we illustrate the detection performance under the power manipulation attack with  $N_{RRH} = 2$  at locations RRH2 and RRH4 and Alice positioned at  $\xi_A = (40 \text{ m}, 30 \text{ m})$ . In the lefthand axis of Fig. 6(a), we show the missed detection probability under the power manipulation strategy for perfect and statistical CSI knowledge at Eve. The righthand axis shows the corresponding power manipulation amplitude  $\eta_E$  for the statistical CSI strategy in (21). We observe that for positions close to RRH4, Eve can achieve close to the optimal success probability

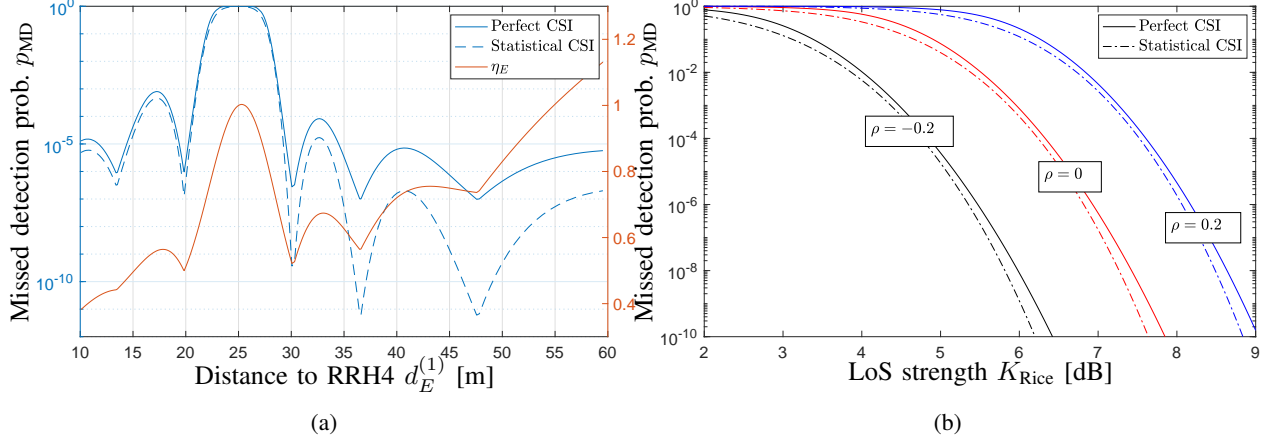


Fig. 6. Detection performance under power manipulation attack for varying CSI knowledge: (a) for varying attack position and (b) for fixed position with varying Rice factor.

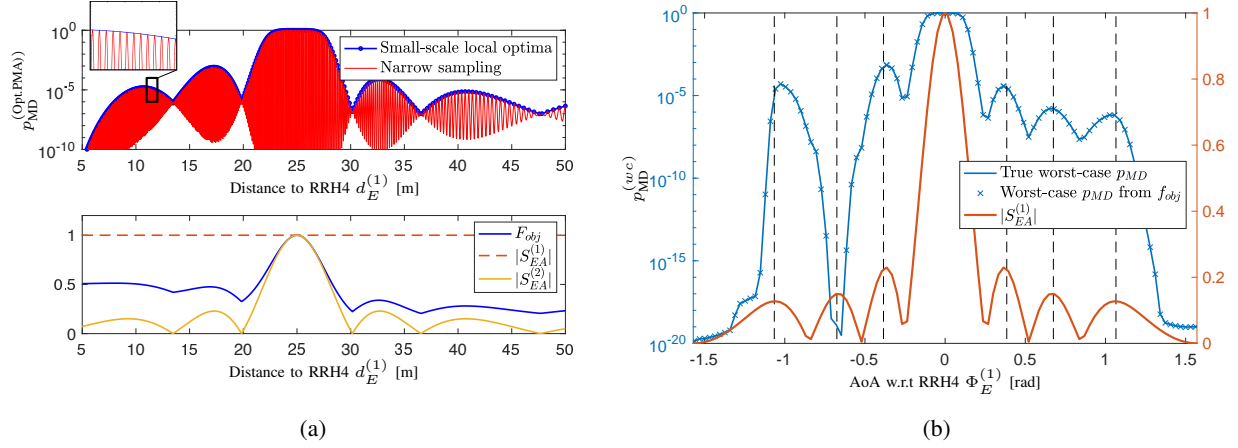


Fig. 7. Missed detection probability under optimal power manipulation for different attack positions along: (a) a line with fixed AoA with respect to RRH4 and (b) a range of AoAs with respect to RRH4 where distance is optimized to obtain the maximum MDP.

with only statistical CSI knowledge. As expected, we can also observe that the required power manipulation amplitude  $\eta_E$  increases with distance since Eve needs to compensate for the higher path-loss compared to Alice's channel. In Fig. 6(b), we show the same missed detection probabilities but for a fixed attack position  $\xi_E = (32 \text{ m}, 30 \text{ m})$  and varying LoS strength in terms of the Rice factor  $K_{Rice}$ . We again observe that Eve can achieve close to the optimal performance with only statistical CSI knowledge. However, we also observe that both probabilities decay rapidly with increased LoS strength.

### C. Optimization of Attacker Position

In Fig. 7 we consider a deployment with  $N_{RRH} = 2$  arrays with  $N_{Rx} = 8$  antennas each, positioned according to RRH2 and RRH4 in Fig. 3. In this figure the LoS strength is  $K_{Rice} = 6$

dB. In Fig. 7(a), both Alice and Eve are centered in front of RRH4 and Eve is varying her distance with respect to this array. Firstly, the upper part of Fig. 7(a) illustrates that, by following the result in Lemma 6, we can appropriately sample the local maxima of  $p_{\text{MD}}^{(\text{Opt.PMA})}$ . We observe that the sampled envelope of the MDP approaches  $1 - p_{\text{FA}} \approx 1$  when the distance comes close to 25 m since this means that Eve is very close to Alice's position. The lower part illustrates the objective function  $F_{\text{obj}}(\xi_E)$  in (26) and the two angular response inner products  $S_{AE}^{(1)}$  and  $S_{AE}^{(2)}$  given by (24). We observe that the envelope of the MDP curve (in the upper plot) closely resembles the shape of the objective function (in the lower plot) which justifies the use of  $F_{\text{obj}}$  for optimization in our heuristic approach.  $S_{AE}^{(2)}$  follows the angular response for the second array (i.e., RRH4) and illustrates that the best attack positions on this straight line are located at the intersections with the side lobes of the second array. The fact that  $S_{AE}^{(1)}$  remains constant is expected since Eve is moving along the main lobe of the first array (i.e., RRH3) and does not change the AoA with respect to this array.

In exactly the same scenario as above, Fig. 7(b) shows the worst-case MDP along a given AoA with respect to RRH4. In this figure, the worst-case MDP was obtained by exhaustive search along a straight line for each AoA. The solid line indicates the true maximum MDP along the corresponding AoA. The cross markers illustrate the corresponding MDP obtained by maximizing  $F_{\text{obj}}(\xi_E)$  along the corresponding AoA. Their agreement again illustrates that the heuristic approach, that optimizes  $F_{\text{obj}}(\xi_E)$ , provides valid results. Moreover, we can observe that if Eve is not allowed close to Alice (e.g.,  $\Phi_E^{(1)} > 0.2$  rad) there is a local optimal AoA around  $\Phi_E^{(1)} = 0.4$  (the first local maxima for positive  $\Phi_E^{(1)}$ ) that agrees well with the first side lobe of RRH4.

Fig. 8 exemplifies a result of the optimization algorithm proposed in Section IV-E over the entire deployment area. For this example, we have assumed  $K_{\text{Rice}} = 6$  dB,  $p_{\text{FA}} = 10^{-2}$ ,  $\rho = 0$ ,  $N_{\text{Rx}} = 8$ , and  $N_{\text{RRH}} = 2$ . The red-shaded regions in Fig. 8(a) mark the areas that are searched, i.e., main lobes and intersections of side lobes. We have defined the allowed region  $\mathcal{R}$  as positions further than 6 m from Alice and 3 m from the RRHs. In this map, we show the obtained local optimal positions, and the global optimal position obtained by our approach compared to the true global optimal position obtained by an exhaustive search. We can see that the heuristic approach finds the true worst-case position that lies within one of the search areas along the main lobe of RRH1. For this scenario, the worst-case MDP is around  $10^{-3}$ . Fig. 8(b) shows the objective function values and corresponding MDP for each of the candidate positions. We can



observe that the positions with larger objective function values are, in fact, the positions with higher MDP.

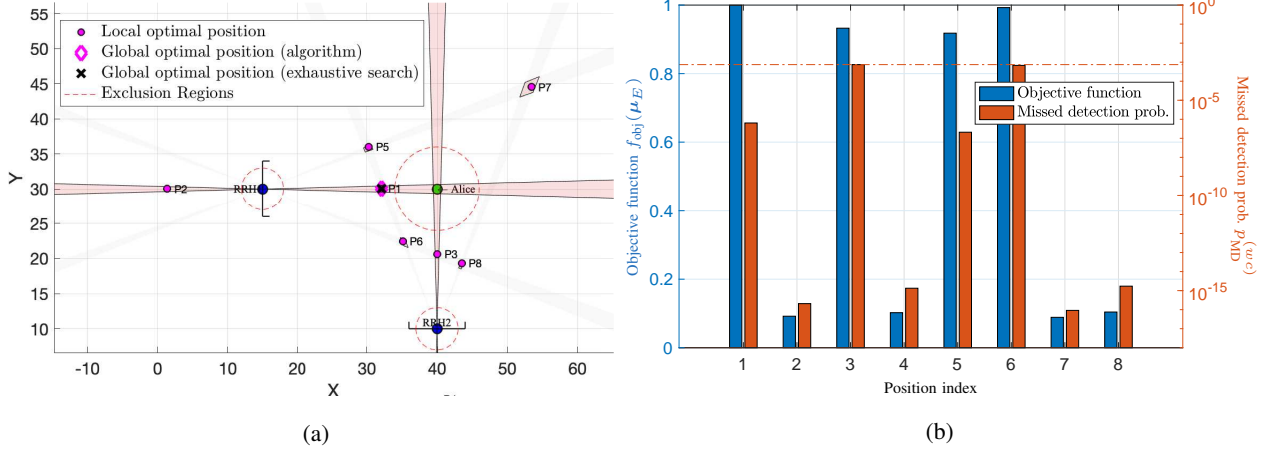


Fig. 8. Example of optimization for Scenario A: (a) map over considered deployment and marked positions; (b) the corresponding objective function values and MDPs.

In Fig. 9, we illustrate heat-maps of the log-MDP for four different deployment scenarios. It is important to note that in every deployment the total number of deployed antennas is fixed to  $N_{RRH}N_{Rx} = 16$ . We have truncated the MDP values so that the completely yellow regions correspond to a MDP less than  $10^{-15}$ . In the second deployment (i.e., with  $N_{RRH} = 2, N_{Rx} = 8$ ), it is possible to see that many side lobe intersections are associated with slightly increased MDP values indicated by blue regions.

#### D. Comparison of Deployment Scenarios

In Table I, we summarize the results from evaluating the search algorithm for different deployment scenarios. For these results we applied an exclusion region of points within 6 m from

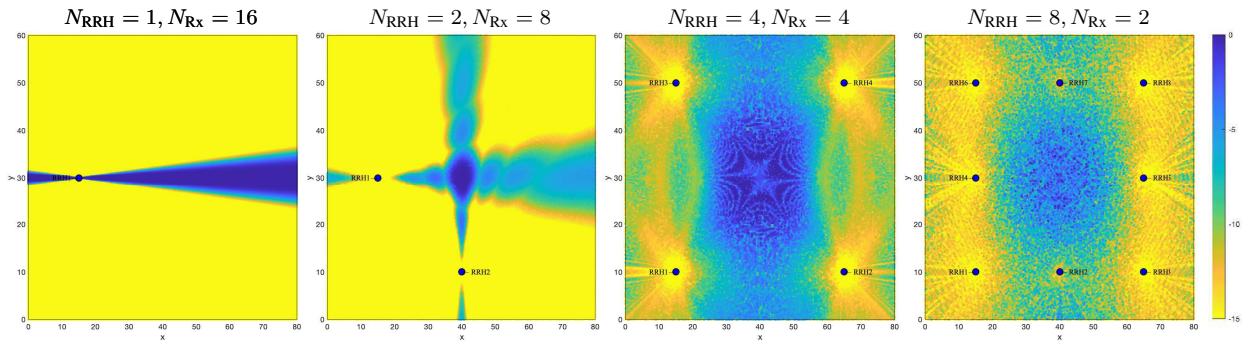


Fig. 9. Heat-maps of log-MDP  $\log_{10}(p_{MD}^{(Opt. PMA)})$  for different deployment scenarios.

Scenario	$N_{\text{RRH}}$	$N_{\text{Rx}}$	Tot. # antennas	$p_{\text{MD}}^{(\text{Opt. Position})}$	Coverage	# Search pos.	# Small-scale local optima
A	2	8	16	7.469913e-04	99,96%	9730 (3,5%)	278263
B	4	4	16	9.377572e-01	97,96%	40649 (10,1%)	401358
C	8	2	16	6.260576e-01	99,77%	105431 (29,9%)	352295
D	2	6	12	7.367218e-02	97,84%	5923 (2,1%)	277892
E	3	4	12	9.558150e-01	94,96%	28665 (7,3%)	394787
F	4	3	12	9.803737e-01	92,23%	55750 (13,9%)	400514
G	6	2	12	9.266438e-01	96,74%	96962 (27,2%)	356388

TABLE I. Summary of results for deployment scenarios A-G.

Alice and within 3 m from each RRH. For each scenario, the table shows the obtained worst-case MDP, the area coverage in percent, number of small-scale sampling positions searched by the algorithm, and the total number of small-scale sampling positions in the entire deployment area. Area coverage is here defined as the percentage of points with  $p_{\text{MD}}^{(\text{Opt. PMA})} < 10^{-4}$ .

For comparison, consider that an exhaustive search with sampling resolution of  $\lambda_c/10 = 0.0125$  m would result in a complexity on the order of  $10^7$  positions in the considered  $80 \text{ m} \times 60 \text{ m}$  area. From Table I, we see that the final number of search positions are in orders ranging from  $10^3$  (Scenario A and D) to  $10^5$  (Scenario C), representing a significant complexity reduction compared to the exhaustive search. This reduction is generally larger for less distributed scenarios (e.g. only 3.5% of all the local optima are searched for Scenario A). The reason for this is twofold: (i) with fewer RRHs, there are fewer main lobes and intersection regions in total, and (ii) with more antennas per array, the beams of each RRH are more directed, and thus, the main lobe and intersection areas become smaller.

For the considered settings, the  $N_{\text{RRH}} = 2$  deployments (scenario A and D) provide the lowest worst-case MDP for the given total number of antennas. These scenarios also result in the highest coverage. We can also observe that the more distributed scenarios  $N_{\text{RRH}} > 2$  all result in a worst-case MDP close to 1. While noting that this observation depends on the choice of exclusion region, which in this case is a 6 m disc around Alice, these results indicate that distributing antennas to more than  $N_{\text{RRH}} = 2$  locations provides no additional benefits in terms of worst-case missed detection probability. That is, for a  $N_{\text{RRH}} = 2$  deployment, one should rather invest in adding antennas to the existing RRHs than in distributing the antennas further.

### *E. Discussion*

The numerical results have illustrated how the obtained performance guarantees depends on deployment strategy, exclusion region, LoS strength, and fading correlation. In reality, only some of these parameters can be influenced for security purposes. Channel characteristics such as LoS strength are obviously mostly determined by the environment where the system is deployed. Here, we can only conclude that the studied authentication scheme would be better suitable where strong LoS channels are expected (e.g., in an open industry hall or a road side). Fading correlation, which according to our results improves detection performance, can to some extent be influenced through system design by densely spaced arrays; however, note that in our model such a modification would also affect the normalized antenna separation, and consequently, the beam-forming pattern.

The studied deployment scenarios indicate some lessons on how RRH positioning could be influenced during system design for security purposes. Firstly, we have observed that a single RRH deployment is very vulnerable to a power manipulation attack as long as the attacker is positioned along the same AoA as the legitimate device (see e.g., first plot in Fig. 9). With that observation in mind, our results clearly illustrates the benefits of a distributed approach compared to the single RRH scenario. In terms of worst-case MDP, however, our results show no benefits of further distributing the antennas to more than two RRHs, and a comparison of Scenario A and D suggests that narrowing the beams of two existing arrays by adding more antennas is more beneficial than adding additional RRHs. However, note that this generally is a question of what assumptions we make regarding the exclusion region (i.e., how close to the legitimate device can an attacker realistically be expected to come). Compare, for example, the deployment  $N_{\text{RRH}} = 2$  and  $N_{\text{RRH}} = 8$  in Fig. 9 where it can be argued that the 8 RRH deployment would be preferable to protect against attackers close to the edges of the deployment area (e.g., in a case where it is unlikely that an attacker can get physically close to the legitimate device). To fully answer such questions, further assumptions on the type of system are needed like, e.g., if the system is publicly deployed, if devices are mobile or stationary, and if it is likely that an internal device could be an attacker, etc.

## VI. CONCLUSION

In this paper, we have presented methods for analyzing worst-case detection performance bounds for physical layer authentication in a wireless network with a distributed architecture.

This analysis is motivated by the problem of providing strict guarantees that are required if physical layer authentication is to be considered as a viable security technique in future mission-critical communications. To address this problem, we have defined two different attack strategies: the power manipulation attack and optimal position attack and provided mathematical tools for finding the worst-case missed detection performance under the optimal strategies.

Our results indicate that a distributed architecture can significantly reduce the worst-case missed detection probability for fixed number of antennas. However, for the considered deployment scenario, our worst-case analysis has shown no performance improvements from distributing antennas on more than two RRHs. That is, for a distributed system with two remote radio heads, instead of adding a third array one should rather use additional antennas to narrow the beams of the existing two arrays. Moreover, we note that the authentication scheme in the distributed RRH architecture remains to be analyzed from a delay perspective.

## REFERENCES

- [1] R. Chen, C. Li, S. Yan, R. Malaney, and J. Yuan, "Physical layer security for ultra-reliable and low-latency communications," *IEEE Wireless Communications*, vol. 26, no. 5, pp. 6–11, October 2019.
- [2] A. Weinand, R. Sattiraju, M. Karrenbauer, and H. D. Schotten, "Supervised learning for physical layer based message authentication in URLLC scenarios," in *IEEE 90th Vehicular Technology Conference*, Sep. 2019, pp. 1–7.
- [3] L. Xiao, L. Greenstein, N. Mandayam, and W. Trappe, "Fingerprints in the ether: Using the physical layer for wireless authentication," in *IEEE International Conference on Communications*, June 2007, pp. 4646–4651.
- [4] A. Abdelaziz, R. Burton, and C. E. Koksall, "Poster: Message authentication and secret key agreement in vanets via angle of arrival," in *IEEE Vehicular Networking Conference*, 2016, pp. 1–2.
- [5] N. Gao, Q. Ni, D. Feng, X. Jing, and Y. Cao, "Physical layer authentication under intelligent spoofing in wireless sensor networks," *Signal Processing*, vol. 166, p. 107272, 2020. [Online]. Available: <http://www.sciencedirect.com/science/article/pii/S0165168419303263>
- [6] A. Weinand, M. Karrenbauer, R. Sattiraju, and H. Schotten, "Application of machine learning for channel based message authentication in mission critical machine type communication," in *European Wireless Conference*, May 2017, pp. 1–5.
- [7] A. Weinand, M. Karrenbauer, J. Lianghai, and H. D. Schotten, "Physical layer authentication for mission critical machine type communication using Gaussian mixture model based clustering," in *IEEE Vehicular Technology Conference*, June 2017, pp. 1–5.
- [8] W. Hou, X. Wang, J.-Y. Chouinard, and A. Refaey, "Physical layer authentication for mobile systems with time-varying carrier frequency offsets," *IEEE Transactions on Communications*, vol. 62, no. 5, pp. 1658–1667, May 2014.
- [9] S. Jana and S. K. Kasera, "On fast and accurate detection of unauthorized wireless access points using clock skews," *IEEE Transactions on Mobile Computing*, vol. 9, no. 3, pp. 449–462, March 2010.
- [10] B. Danev and S. Capkun, "Transient-based identification of wireless sensor nodes," in *2009 International Conference on Information Processing in Sensor Networks*, April 2009, pp. 25–36.
- [11] S. Hussain, "Using received signal strength indicator to detect node replacement and replication attacks in wireless sensor networks," in *Proceedings of SPIE - The International Society for Optical Engineering*, vol. 7344, 04 2009.

- [12] A. Abdelaziz, C. E. Koksall, F. Barickman, R. Burton, J. Martin, and J. Weston, "Enhanced authentication based on angle of signal arrivals," *IEEE Transactions on Vehicular Technology*, pp. 1–1, 2019.
- [13] P. Baracca, N. Laurenti, and S. Tomasin, "Physical layer authentication over MIMO fading wiretap channels," *IEEE Transactions on Wireless Communications*, vol. 11, no. 7, pp. 2564–2573, July 2012.
- [14] P. L. Yu, J. S. Baras, and B. M. Sadler, "Physical-layer authentication," *IEEE Transactions on Information Forensics and Security*, vol. 3, no. 1, pp. 38–51, March 2008.
- [15] M. K. Shukla, A. Trivedi, and O. J. Pandey, "Physical layer authentication for mobile terminals over MIMO fading wiretap channels," in *International Conference on Advances in Computing, Communications and Informatics (ICACCI)*, Aug 2013, pp. 638–642.
- [16] L. Xiao, T. Chen, G. Han, W. Zhuang, and L. Sun, "Game theoretic study on channel-based authentication in MIMO systems," *IEEE Transactions on Vehicular Technology*, vol. PP, no. 99, pp. 1–1, 2017.
- [17] L. Senigagliaesi, M. Baldi, and E. Gambi, "Performance of statistical and machine learning techniques for physical layer authentication," *CoRR*, Jan 2020. [Online]. Available: <https://arxiv.org/abs/2001.06238>
- [18] H. Forssell, R. Thobaben, H. Al-Zubaidy, and J. Gross, "On the impact of feature-based physical layer authentication on network delay performance," in *IEEE Global Communications Conference*, Dec 2017, pp. 1–6.
- [19] H. Forssell, R. Thobaben, and J. Gross, "Performance analysis of distributed simo physical layer authentication," in *IEEE International Conference on Communications*, May 2019, pp. 1–6.
- [20] H. Forssell, R. Thobaben, H. Al-Zubaidy, and J. Gross, "Physical layer authentication in mission-critical mtc networks: A security and delay performance analysis," *IEEE Journal on Selected Areas in Communications*, vol. 37, no. 4, pp. 795–808, April 2019.
- [21] L. Xiao, L. Greenstein, N. Mandayam, and W. Trappe, "Using the physical layer for wireless authentication in time-variant channels," *IEEE Transactions on Wireless Communications*, vol. 7, no. 7, pp. 2571–2579, July 2008.
- [22] T. Y. Al-Naffouri, M. Moinuddin, N. Ajeeb, B. Hassibi, and A. L. Moustakas, "On the distribution of indefinite quadratic forms in gaussian random variables," *IEEE Transactions on Communications*, vol. 64, no. 1, pp. 153–165, Jan 2016.

## APPENDIX

### A. Optimal Power Manipulation Strategy

Recall that  $d(\rho_E e^{j\varphi_E} \mathbf{h}_E)$  is the discriminant function that the attacker is trying to minimize. We note that by using a Cholesky factorization  $\Sigma_A^{-1} = \mathbf{Q}_A^\dagger \mathbf{Q}_A$ , we can write

$$\begin{aligned} d(\rho_E e^{j\varphi_E} \mathbf{h}_E) &= \|\rho_E e^{j\varphi_E} \mathbf{h}_E - \boldsymbol{\mu}_A\|_{\Sigma_A^{-1}}^2 = 2\|\mathbf{Q}_A(\rho_E e^{j\varphi_E} \mathbf{h}_E - \boldsymbol{\mu}_A)\|^2 \\ &= 2(\rho_E^2 \|\mathbf{Q}_A \mathbf{h}_E\|^2 + \|\mathbf{Q}_A \boldsymbol{\mu}_A\|^2 - 2\rho_E \Re\{e^{j\varphi_E} (\mathbf{Q}_A \boldsymbol{\mu}_A)^\dagger \mathbf{Q}_A \mathbf{h}_E\}). \end{aligned} \quad (34)$$

Taking the derivative w.r.t.  $\rho_E$ , we get  $\frac{\partial}{\partial \rho_E} d(\rho_E e^{j\varphi_E} \mathbf{h}_E) = 4\rho_E \|\mathbf{Q}_A \mathbf{h}_E\|^2 - 4\Re\{e^{j\varphi_E} (\mathbf{Q}_A \boldsymbol{\mu}_A)^\dagger \mathbf{Q}_A \mathbf{h}_E\}$  and, hence,  $\rho_E^*$  such that  $\frac{\partial}{\partial \rho_E} d(\rho_E e^{j\varphi_E} \mathbf{h}_E) = 0$  results in

$$\rho_E^* = \frac{\Re\{e^{j\varphi_E} (\mathbf{Q}_A \boldsymbol{\mu}_A)^\dagger \mathbf{Q}_A \mathbf{h}_E\}}{\|\mathbf{Q}_A \mathbf{h}_E\|^2} = \frac{\Re\{e^{j\varphi_E} \boldsymbol{\mu}_A^\dagger \Sigma_A^{-1} \mathbf{h}_E\}}{\mathbf{h}_E^\dagger \Sigma_A^{-1} \mathbf{h}_E}. \quad (35)$$

Plugging (35) into (34), we get

$$d(\rho_E^* e^{j\varphi_E} \mathbf{h}_E) = 2 \left( \boldsymbol{\mu}_A^\dagger \boldsymbol{\Sigma}_A^{-1} \boldsymbol{\mu}_A - \frac{\Re\{e^{j\varphi_E} \boldsymbol{\mu}_A^\dagger \boldsymbol{\Sigma}_A^{-1} \mathbf{h}_E\}^2}{\mathbf{h}_E^\dagger \boldsymbol{\Sigma}_A^{-1} \mathbf{h}_E} \right). \quad (36)$$

Clearly,  $d(\rho_E^* e^{j\varphi_E} \mathbf{h}_E)$  is minimized when  $e^{j\varphi_E} \boldsymbol{\mu}_A^\dagger \boldsymbol{\Sigma}_A^{-1} \mathbf{h}_E$  is real-valued so that  $\Re\{e^{j\varphi_E} \boldsymbol{\mu}_A^\dagger \boldsymbol{\Sigma}_A^{-1} \mathbf{h}_E\} = |\boldsymbol{\mu}_A^\dagger \boldsymbol{\Sigma}_A^{-1} \mathbf{h}_E|$ , which is obtained by setting  $\varphi_E^* = -\arg\{\boldsymbol{\mu}_A^\dagger \boldsymbol{\Sigma}_A^{-1} \mathbf{h}_E\}$ . Plugging  $\varphi_E^*$  into (36) and rearranging yields (6) which completes the proof.

### B. Integral Representation

Introducing,  $\bar{\mathbf{h}}_E = \mathbf{b} + \mathbf{h}$ , we can integrate over the PDF of  $\mathbf{h} \sim \mathcal{CN}(\mathbf{0}, \mathbf{I})$  according to

$$p_{\text{MD}}^{(\text{wc})}(T) = \int_{-\infty}^{\infty} \frac{1}{\pi^N} e^{-\mathbf{h}^\dagger \mathbf{h}} \mathcal{U}((\mathbf{b} + \mathbf{h})^\dagger \mathbf{A}(\mathbf{b} + \mathbf{h})) d\mathbf{h}, \quad (37)$$

where  $\mathcal{U}(\cdot)$  denotes the Heaviside step function. By using the Laplace representation<sup>3</sup>  $1 - \mathcal{U}(x) = -\frac{1}{2\pi} \int_{-\infty}^{\infty} \frac{e^{-x(j\omega - \beta)}}{j\omega - \beta} d\omega$  valid for  $\beta > 0$ , we can rewrite (37) as

$$\int_{-\infty}^{\infty} \frac{1}{\pi^N} e^{-\mathbf{h}^\dagger \mathbf{h}} \left[ -\frac{1}{2\pi} \int_{-\infty}^{\infty} \frac{e^{-(j\omega - \beta)(\mathbf{b} + \mathbf{h})^\dagger \mathbf{A}(\mathbf{b} + \mathbf{h})}}{j\omega - \beta} d\omega \right] d\mathbf{h} = -\frac{1}{2\pi^{N+1}} \int_{-\infty}^{\infty} \int_{-\infty}^{\infty} \frac{e^{-\mathbf{h}^\dagger \mathbf{h} - (\mathbf{b} + \mathbf{h})^\dagger (j\omega - \beta) \mathbf{A}(\mathbf{b} + \mathbf{h})}}{j\omega - \beta} d\omega d\mathbf{h}. \quad (38)$$

Using the decomposition  $\mathbf{A} = \mathbf{U} \mathbf{D} \mathbf{U}^\dagger$ , the transformations  $\tilde{\mathbf{h}} = \mathbf{U}^\dagger \mathbf{h}$  and  $\bar{\mathbf{b}} = \mathbf{U}^\dagger \mathbf{b}$ , and the fact that  $d\mathbf{h} = d\tilde{\mathbf{h}}$ , we can write (38) as

$$-\frac{1}{2\pi^{N+1}} \int_{-\infty}^{\infty} \int_{-\infty}^{\infty} \frac{e^{-\tilde{\mathbf{h}}^\dagger \tilde{\mathbf{h}} - (\tilde{\mathbf{h}} + \bar{\mathbf{b}})^\dagger (j\omega - \beta) \mathbf{D}(\tilde{\mathbf{h}} + \bar{\mathbf{b}})}}{j\omega - \beta} d\omega d\tilde{\mathbf{h}} = -\frac{1}{2\pi^{N+1}} \int_{-\infty}^{\infty} \int_{-\infty}^{\infty} \frac{e^{-(\tilde{\mathbf{h}} + \bar{\mathbf{b}})^\dagger \mathbf{B}(\tilde{\mathbf{h}} + \bar{\mathbf{b}}) - c(\omega)}}{j\omega - \beta} d\omega d\tilde{\mathbf{h}}, \quad (39)$$

with  $\mathbf{B} = \mathbf{I} + (j\omega - \beta) \mathbf{D}$ ,  $\tilde{\mathbf{b}} = \left( \mathbf{I} + \frac{1}{j\omega - \beta} \mathbf{D}^{-1} \right)^{-1} \bar{\mathbf{b}}$ , and  $c(\omega) = \bar{\mathbf{b}}^\dagger \left( \mathbf{I} + \frac{1}{j\omega - \beta} \mathbf{D}^{-1} \right)^{-1} \bar{\mathbf{b}}$ . We can then integrate out  $\tilde{\mathbf{h}}$  by noting that (39) can be written as

$$-\frac{1}{2\pi} \int_{-\infty}^{\infty} \int_{-\infty}^{\infty} \frac{1}{\pi^N} e^{-(\tilde{\mathbf{h}} + \bar{\mathbf{b}})^\dagger \mathbf{B}(\tilde{\mathbf{h}} + \bar{\mathbf{b}})} d\tilde{\mathbf{h}} \frac{e^{-c(\omega)}}{j\omega - \beta} d\omega = -\frac{1}{2\pi} \int_{-\infty}^{\infty} \frac{e^{-c(\omega)}}{(j\omega - \beta) |\mathbf{I} + (j\omega - \beta) \mathbf{D}|} d\omega, \quad (40)$$

where we have used the fact that the Gaussian integral  $\int_{-\infty}^{\infty} \frac{1}{\pi^N} e^{-(\tilde{\mathbf{h}} + \bar{\mathbf{b}})^\dagger \mathbf{B}(\tilde{\mathbf{h}} + \bar{\mathbf{b}})} d\tilde{\mathbf{h}} = \frac{1}{|\mathbf{B}|}$  is solvable in closed form.

<sup>3</sup>According to [22], it is more convenient to work with  $1 - \mathcal{U}(x)$  when evaluating the complementary CDF.